

1 **Measurement Report: Rapid changes of chemical characteristics and health risks for high**
2 **time-resolved trace elements in PM_{2.5} in a typical industrial city in response to stringent**
3 **clean air actions**

4 Rui Li^{a*}, Yining Gao^a, Yubao Chen^a, Meng Peng^{b c*}, Weidong Zhao^{c*}, Gehui Wang^a, Jiming Hao^b

5 ^a *Key Laboratory of Geographic Information Science of the Ministry of Education, School of*
6 *Geographic Sciences, East China Normal University, Shanghai, 200241, P.R. China*

7 ^b *State Key Joint Laboratory of Environment Simulation and Pollution Control, School of*
8 *Environment, Tsinghua University, Beijing, 100084, P.R. China*

9 ^c *Institute of Energy conservation and Environmental Protection, China Electronic Information*
10 *Industry Development Research Institute, Beijing, 100084, P.R. China*

11 *** Correspondence to:**

12 Prof. Li (rli@geo.ecnu.edu.cn), Dr. Peng (mvponesky@163.com), and Prof. Zhao

13 (zhaoweidong@ccidthinktank.com)

14 **Abstract**

15 Atmospheric trace metals entail significant damages in human health and ecosystem safety, and thus
16 a series of clean air actions have been implemented to decrease the ambient element concentrations.

17 Unfortunately, the impact of these emission control measures on element concentrations in fine
18 particles remains poorly understood. In our study, the random forest (RF) model was applied to

19 distinguish the effects of emission and meteorology to trace elements in PM_{2.5} in a typical industrial
20 city named Tangshan based on a three-year (2017-2020) hourly field observation. The result

21 suggested that the clean air actions have facilitated the dramatic decreases of the deweathered
22 concentrations of Ga, Co, Pb, Zn, and As by 72%, 67%, 62%, 59%, and 54%, respectively. It is

23 attributable to the strict implementation of “coal to gas” strategies and optimization of industrial
24 structure and layout. However, the deweathered levels of Ca (8.3%), Cr (18.5%), and Fe (23%) only

25 displayed minor decreases, indicating that the emission control measures for ferrous metal smelting
26 and vehicle emission were not very effective. The positive matrix factorization (PMF) results

27 suggested that the contribution ratios of biomass burning, non-ferrous metal smelting, coal

28 combustion, ferrous metal smelting, heavy oil combustion, and traffic-related dust changed from
29 33%, 11%, 15%, 13%, 3%, and 25% to 33%, 8%, 8%, 13%, 4%, and 33%, respectively. To date,
30 no significant noncarcinogenic and carcinogenic risks were observed for all of the elements, while
31 both of As and Pb still showed relatively high health damages. It was proposed to further cut down
32 the combustion-related emissions (e.g., As and Pb) because it showed the highest marginal health
33 benefits. Besides, the control of traffic-related emissions might be a key abatement strategy to
34 facilitate the reduction of elements in fine particles.

35 **Keywords:** hourly trace elements; chemical characteristics; health risks; clean air actions; Tangshan

36 **1. Introduction**

37 Along with the rapid economic development and accelerated urbanization, the energy
38 consumption and output of various industrial products worldwide displayed persistent increases,
39 thereby leading to massive emissions of elements especially trace metals into the atmosphere (Tian
40 et al., 2015; Zhu et al., 2020). These elements injected into the atmosphere could pose great threat
41 to the terrestrial and aquatic ecosystem via dry/wet deposition and then endanger human health
42 through the physicochemical transfer and bioaccumulation in food chains (Fernandez et al., 2000;
43 Harmens et al., 2010; Storelli, 2008). For instance, some toxic trace metals including cadmium (Cd),
44 lead (Pb), and mercury (Hg) were often regarded as human carcinogens even in trace amounts
45 (Micheline et al., 2019; Olujimi et al., 2015). Besides, the excessive accumulation of some
46 biological essential elements such as copper (Cu), iron (Fe), and zinc (Zn) could initiate activation
47 of inflammatory cascades in tissues and the induction of biochemical synthesis pathways by
48 catalyzing the generation of reactive oxygen species (ROS) (Alies et al., 2013; Lopez-Cruz et al.,
49 2016; Saffari et al., 2014), though minor enrichment of these elements was beneficial to the human
50 health and plant growth (Oldani et al., 2017). Apart from the health impacts, some transition metals
51 (e.g., Ni, Zn) could catalyze some chemical reactions such as particle-phase sulfate generation and
52 heterogeneous production and removal of gas-phase hydrogen oxide radicals (HO_x) to aggravate the
53 haze formation (Clements et al., 2013; Guo et al., 2014). Therefore, it is highly imperative to
54 recognize the pollution status of elements in the atmosphere, to identify the major sources and then
55 to propose effective control measures to alleviate their negative effects on air pollution and human
56 health especially in some developing countries.

57 In the past decades, hundreds of studies investigated the pollution levels of elements and
58 revealed their sources in various study regions including urban (Das et al., 2018; Duan and Tan,
59 2013; Lyu et al., 2017; Grivas et al., 2018; Clements et al., 2014), marine (Shi et al., 2015; Witt et
60 al., 2006), mountainous (Kang et al., 2016). Most of these studies used filter sampling (one sample
61 or two samples each day) coupled with offline analysis using inductively coupled plasma mass
62 spectrometry (ICP-MS) or inductively coupled plasma-atomic emission spectrometry (ICP-AES) to
63 determine the element concentrations in the atmosphere (Ao et al., 2019; Lin et al., 2016). Although
64 these studies have obtained much valuable information about the occurrence levels and key sources
65 of ambient elements, the low time-resolution data cannot accurately reflect the dynamic
66 transformation and evolution of ambient elements. It was well known that atmospheric emissions,
67 transport and deposition significantly relied on rapidly evolving meteorological conditions (Holden
68 et al., 2016; Rasmussen, 1998), and thus the offline samples inevitably ignored the impacts of
69 environmental shifts with rapid temporality on the atmospheric element concentrations. Moreover,
70 most of current source apportionment studies employed receptor models (positive matrix
71 factorization (PMF)) to determine the potential sources of elements (Jeong et al., 2016; Lyu et al.,
72 2017), and the accuracy of these models was strongly dependent on the sample size and time
73 resolution (Liu et al., 2018b). In this regard, the high time-resolved observation of atmospheric
74 elements provided an unprecedented opportunity to characterize the occurrence levels, identify their
75 major sources, and assess the health impacts.

76 To date, only a few studies applied the high-resolution devices to capture the hourly variability
77 of ambient elements. Prati et al. (2000) firstly used Particle Induced X-ray Emission (PIXE)
78 measurements to measure hourly trace elements in Genoa in Italy. Following this work,
79 D'Alessandro et al. (2003) and Dall'Osto et al. (2013) also employed the same technique to
80 determine the trace metals in Italian towns and Barcelona, respectively. Later on, Jeong et al. (2016)
81 used the Xact metals monitor to reveal the temporal variability of atmospheric elements in Toronto,
82 Canada in summer and winter during 2013-2014. Recently, the Xact metals monitor has begun to
83 be employed in China due to the higher accuracy and convenience. Chang et al. (2018) firstly used
84 the online multi-element analyzer to achieve a one-year near real-time observation of ambient
85 elements in China and found that traffic, nonferrous metal smelting and coal combustion were major

86 sources of atmospheric trace metals. Afterwards, Cui et al. (2019) applied the analyzer to monitor
87 atmospheric elements during a full year, and demonstrated that dust, industry, and biomass burning
88 were the dominant sources of most trace elements in Beijing, accounting for 36%, 10.7%, and 27%
89 of total PM_{2.5} concentration, respectively. Up to date, continuous hourly element observation was
90 only performed less than one year in most of the previous studies, and the long-term temporal
91 variability of absolute concentrations and key pollution sources of atmospheric elements cannot be
92 fully revealed.

93 Since 2013, Chinese government proposed a strict Air Pollution Prevention and Control Action
94 Plan (the Action Plan) across China and the emissions of multiple gaseous pollutants showed
95 significant decreases. In turn, the absolute concentrations and health effects of air pollutants also
96 experienced the rapid changes due to these stringent control measures. Zhang et al. (2019) reported
97 that the population-weighted annual mean PM_{2.5} concentration decreased from 62 to 42 µg/m³
98 during 2013-2017 and reduced PM_{2.5}-attributable premature deaths by 0.4 million due to the impact
99 of the Action Plan. Shortly after that, Geng et al. (2019) estimated that the population-weighted
100 mean concentrations of SO₄²⁻, NO₃⁻, and NH₄⁺ in PM_{2.5} decreased from 11.1, 13.8, and 7.4 µg/m³ to
101 6.7, 13.1, and 5.8 µg/m³, respectively, during the same period. Nevertheless, the impact of the Action
102 Plan on trace elements in fine particles still remained poorly understood. Especially, the knowledge
103 about the variation of source apportionment and health risks for trace elements response to the
104 Action Plan was extremely limited. Moreover, most of the previous studies only utilized the original
105 concentrations to analyze the impact of the clean air policy (He et al., 2021; Xiao et al., 2020). It
106 was well known that the pollutant concentrations in the atmosphere were affected by meteorology
107 and anthropogenic emissions simultaneously (Li et al., 2021), and the use of original element
108 concentrations alone cannot assess the unique contribution of emission reduction to the air pollutants.
109 Thus, it is urgently needed to remove the effect of meteorology and accurately capture the
110 independent influence of the Action Plan on the chemical characteristics, source apportionment, and
111 health risks of trace elements. Such knowledge is critical to design effective air pollution mitigation
112 strategies in the near future.

113 As a heavily industrialized city located in the North China Plain (NCP), Tangshan possesses
114 many energy-intensive industries including coal-fired power plants, non-ferrous smelting industries,

115 textiles, building materials, chemical engineering, and papermaking industries (Ren et al., 2011).
116 Intensifying industrial development and urbanization aggravated local air quality. Previous studies
117 performed in Tangshan focused on the trace metals in soils and dusts (Cui et al., 2020; Song et al.,
118 2011), whereas no study analyzed the long-term and high-resolution variabilities of atmospheric
119 elements. Since 2013, many emission control measures such as the establishment of desulfurization
120 and denitration facilities for the coal-fired power sector have been strictly implemented in Tangshan
121 (Ma et al., 2019). Especially after 2017, the coal to gas project has started to be implemented in
122 Tangshan and the energy structure underwent significant change (Wang et al., 2020b). In response
123 to substantial pollution control policies, the chemical compositions and major sources of trace
124 elements might show corresponding change. Here, we conducted a near real-time measurement of
125 atmospheric elements in PM_{2.5} using a Xact multi-metals analyzer in Tangshan, China, during
126 September 2017 to August 2020. The primary objectives of our study were to (1) determine the
127 occurrence levels of elements in PM_{2.5} of Tangshan; (2) to analyze the seasonal and intra-week
128 variations of atmospheric elements and to distinguish the separate contributions of emission and
129 meteorology to these species; (3) to quantify the changes of major sources for atmospheric elements
130 during this period; (4) to assess the changes of health risks in response to these pollution control
131 measures.

132 **2. Material and methods**

133 2.1 Sampling site

134 The sampling site (39.66°N, 118.18°E) is situated on the rooftop (~20 m above the ground) of a
135 building in the urban district of Tangshan and no high buildings spread around within 100 m range.
136 The sampling site is close to some major roads including the Airport Road, Huayan North Road,
137 and Changhong Road. A large number of commercial streets and recreation facility surround the
138 site. Although no big industrial point source was closely adjacent to the sampling site, many
139 potential pollution sources were located more than 15 km away from the site. For instance, the Beihu
140 industrial region is located about 15 km in the eastern direction of the site. Some large iron steel
141 industries and nonferrous/ferrous smelting industries were located on the north of sampling site
142 (more than 30 km). Besides, most of the large petrochemical industries, coal-fired power plants, and
143 shipping industries focus on the Caofeidian and Haigang developing zones, both of which were

144 located about 50 km in the South area of the sampling site. The detailed location is depicted in
145 Figure 1.

146 2.2 Instrumentation

147 Hourly mass concentrations of 22 elements, including Ag, As, Au, Ca, Co, Cu, Cd, Cr, Fe, Ga,
148 Hg, K, Mn, Ni, Pb, Pd, Sb, Se, Sn, Tl, V, and Zn in PM_{2.5} were determined continuously by an online
149 multi-element analyzer (Model Xact 625, Cooper Environment Service, USA) (Table S1). The
150 sample air is drawn through a small spot on the tape where the PM_{2.5} was collected at a flow rate of
151 16.7 L min⁻¹ during September 2017-August 2020. An internal Pd pod is utilized as an internal
152 standard to determine the stability of the instrument. Tl was removed from the datasets because over
153 95% of their concentrations were below the limit of detection (LOD) (Table S2). Au, Cd, Sn and Sb
154 were also excluded from the datasets because over 50% of the concentrations for these metals were
155 below the LOD. To validate the reliability of the online multi-element analyzer, many previous
156 studies used the filter sampling coupled with ICP-MS and ICP-AES to determine the daily
157 concentrations of elements and confirmed that the online device showed good agreement with the
158 filter sampling (Furger et al., 2017; Tianxue et al., 2006). Hourly averaged meteorological
159 parameters including air temperature (T), relative humidity (RH), air pressure (P), wind direction
160 (WD), and wind speed (WS) during the sampling period were measured by a weather station with
161 sonic anemometer (150WX, Airmar, Milford, NH, USA). The hourly mass concentration of PM_{2.5}
162 was determined by a particulate monitor (Thermo, FH62C-14). The routine procedures, including
163 the daily zero or standard calibration, span and range check, station environmental control and staff
164 certification, followed the Technical Guideline of Automatic Stations of Ambient Air Quality in
165 Tangshan based on the national specification HJ/T193-2005, which was revised based on the
166 technical guidance established by the US EPA. Quality Assurance and Quality Control (QA/QC) for
167 the Xact measurements was implemented throughout the sampling period. The internal Pd upscale
168 value was recorded after daily programmed test for the instrument.

169 2.3 Deweathered model development

170 The concentrations of air pollutants were affected by meteorological parameters and emissions
171 simultaneously. In order to separate the contributions of emissions, the impacts of meteorological
172 conditions must be eliminated. In this study, a typical machine-learning model named random forest

173 (RF) approach was applied to distinguish the effects of emissions and meteorological conditions
174 (Chen et al., 2018). All of the trace elements in PM_{2.5} were treated as the dependent variables. The
175 time predictors (year, day of year (DOY), day of week (DOW), hour of day (HOY)) and
176 meteorological factors including air temperature (T), relative humidity (RH), wind speed (WS),
177 wind direction (WD), and air pressure (P) were regarded as the predictors (Figure S1). The original
178 dataset was randomly classified into a training dataset (80% of input dataset) for developing the RF
179 model and the remained one was treated as the test dataset. After the building of the RF model, the
180 deweathered technique was employed to predict the concentrations of trace elements at a specific
181 time point. The deweathered element concentrations served as the concentrations contributed by
182 emission alone. The differences between the original element concentrations and the deweathered
183 element concentrations were regarded as the concentrations contributed by meteorology. Many
184 statistical indicators including R² value, root-mean-square error (RMSE), and mean absolute error
185 (MAE) were regarded as the major indicators to evaluate the RF modelling accuracy. The RF model
186 with the 5-fold cross-validation R² value less than 0.5 was considered to be an unconvincing result
187 and cannot reflect the impacts of emission and meteorology on air pollutants accurately because
188 more than 50% variability of the training model cannot be appropriately explained. After the model
189 evaluation, only the trace elements with the cross-validation R² values larger than 0.5 were selected
190 to estimate the respective contributions of emission and meteorology to the total element
191 concentrations.

192 2.4 PMF model

193 As a typical receptor model applied to source apportionment, the PMF 5.0 version was used to
194 identify the major origins of the atmospheric elements and to determine the contribution ratio of
195 each source to these elements (Norris et al., 2014). The objective of PMF is to solve the issues of
196 chemical mass balance between the measured concentration of each element and its source
197 contributions by decomposing the input matrix into factor contributions and factor profiles. The
198 detailed equation is shown in Eq. (1). Besides, the contribution of each source for an individual
199 element must be non-negative because no sample has a negative source contribution. In brief, the
200 basic principle of PMF is to calculate the least object function Q when the g_{ik} must be a positive-
201 definite matrix based on Eq. (2) (Paatero and Tapper, 1994; Reff et al., 2007).

202
$$x_{ij} = \sum_{k=1}^p g_{ik} f_{kj} + e_{ij} \quad (1)$$

203
$$Q = \sum_{i=1}^n \sum_{j=1}^m \left[\frac{x_{ij} - \sum_{k=1}^p g_{ik} f_{kj}}{u_{ij}} \right]^2 \quad (2)$$

204 where x_{ij} and e_{ij} denote the concentration and uncertainty of the j th element, respectively. g_{ik}
 205 represents the contribution ratio of the k th source to the i th sample, f_{kj} represents the ratio of the j th
 206 element in the k th source, and e_{ij} indicates the residual of the j th element in the i sample. The
 207 uncertainties associated with factor profiles were evaluated using three error calculation methods
 208 including the bootstrap (BS) method, displacement (DISP) analysis, and the combination method
 209 of DISP and BS (BS-DISP). For the BS method, 100 runs were performed and the result has been
 210 believed to be valid since all of the factors showed a mapping of above 90%. DISP analysis also
 211 confirmed that the solution was considered to be stable because the observed drop in the Q value
 212 was less than 0.1% and no factor swap occurred. For the BS-DISP analysis, the solution has been
 213 verified to be useful because the observed drop in the Q value was less than 0.5%. Furthermore,
 214 both of the results from BS and BS-DISP did not suggest any asymmetry or rotational ambiguity
 215 for all of the factors (Manousakas et al., 2017; Taghvaei et al., 2018).

216 **2.5 Health risk assessment of trace metals in $PM_{2.5}$**

217 As a typical industrial city, Tangshan possesses a large number of residents and poor air quality.
 218 Therefore, the residents in Tangshan might suffer from severe exposure risks of trace metals. In our
 219 work, the carcinogenic and non-carcinogenic risks of trace metals in $PM_{2.5}$ were evaluated based on
 220 some statistical threshold proposed by the International Agency for Research on Cancer (IARC).
 221 Based on the criterion of the IARC, As, Ni, Cr, and Pb were considered to be carcinogenic to humans.

222 The carcinogenic and non-carcinogenic risks induced by metal exposure for adults and children
 223 were evaluated based on the carcinogenic risks (CR) and hazard quotient (HQ). The formulas for
 224 calculating ADD, CR, and HQ are as follows:

225
$$ADD = (C \times InhR \times EF \times ED) / (BW \times AT) \quad (3)$$

226
$$HQ = ADD / RfD \quad (4)$$

227
$$CR = ADD \times CSF \quad (5)$$

228 where C ($mg\ m^{-3}$) denotes the concentration of the corresponding trace metal in $PM_{2.5}$; $InhR$ is the

229 respiratory rate; EF represents the annual exposure frequency (d y^{-1}); ED is the exposure duration
230 (year); BW is the average body weight (kg); AT denotes the average exposure time (d); ADD means
231 the daily intake (mg/kg/day) of trace metals; RfD represents the reference dose ($\text{mg kg}^{-1} \text{d}^{-1}$),
232 calculated with reference concentrations; CSF is the cancer slope factor (kg d mg^{-1}). The potential
233 non-carcinogenic risk of the trace metal might be high when HQ was above 1.0, whereas the health
234 risk is not obvious when HQ is below 1.0. The carcinogenic risk of each trace metal is evaluated
235 based on whether CR is higher than 10^{-4} .

236 **3. Results and discussion**

237 3.1 Occurrence levels and inter-annual variations of original element concentrations

238 The total mass concentrations of 16 elements in $\text{PM}_{2.5}$ of Tangshan varied between 230 ng/m^3
239 to 20000 ng/m^3 , with the average value (\pm standard deviation) of $3100 \pm 900 \text{ ng/m}^3$. The total
240 element concentrations in Tangshan accounted for 5.7% of the total mass concentrations of $\text{PM}_{2.5}$,
241 which was slightly higher than those in Beijing (4.7%) and Qingdao (4.0%), and significantly higher
242 than that in Shanghai (1.80%) (Chang et al., 2018; Cui et al., 2019). As depicted in Figure 2, the
243 concentrations of these elements followed the order of $\text{K} (1400 \pm 950 \text{ ng/m}^3) > \text{Fe} (880 \pm 590$
244 $\text{ ng/m}^3) > \text{Ca} (330 \pm 270 \text{ ng/m}^3) > \text{Zn} (320 \pm 160 \text{ ng/m}^3) > \text{Pb} (58 \pm 36 \text{ ng/m}^3) > \text{Mn} (54 \pm 32 \text{ ng/m}^3) >$
245 $\text{Cu} (22 \pm 19 \text{ ng/m}^3) > \text{As} (15.3 \pm 11.0 \text{ ng/m}^3) > \text{Se} (6.5 \pm 5.3 \text{ ng/m}^3) > \text{V} (4.0 \pm 3.6 \text{ ng/m}^3) > \text{Cr} (2.8$
246 $\pm 2.2 \text{ ng/m}^3) > \text{Ag} (2.8 \pm 2.1 \text{ ng/m}^3) > \text{Ni} (2.2 \pm 1.8 \text{ ng/m}^3) > \text{Hg} (1.5 \pm 0.8 \text{ ng/m}^3) > \text{Ga} (0.9 \pm 0.7$
247 $\text{ ng/m}^3) > \text{Co} (0.7 \pm 0.2 \text{ ng/m}^3)$. Among all of these elements, K, Fe, Zn, and Ca were the most
248 abundant species, accounting for 95% of the total elements in $\text{PM}_{2.5}$. The remaining element
249 concentrations only accounted for less than 6% of the total element concentrations, which was
250 similar to in previous studies (Chang et al., 2018; Cui et al., 2019). Nearly all of the trace elements
251 in Tangshan, Beijing, Qingdao, and Shanghai were significantly lower than those in Zibo during
252 2006-2007 (Table S3). It suggested that the trace elements in China experienced marked decreases
253 in the past decades (Zhang et al., 2018). Compared with some cities in some developed countries,
254 all of the trace element concentrations were significantly higher than those in London and Toronto.
255 Moreover, the concentrations of K, Ca, V, Cr, Mn, and Fe in Tangshan were higher than those in
256 Venice, Italy.

257 Due to the higher exposure risk and great threat to human health, it is necessary to compare the

258 trace metal concentrations with the risk threshold proposed by many organizations or countries. As
259 shown in Table 1, we have collected many risk thresholds in different countries and found that the
260 Hg ($1.5 \pm 0.8 \text{ ng/m}^3$), Ni ($2.2 \pm 1.8 \text{ ng/m}^3$), and Pb concentrations ($58 \pm 36 \text{ ng/m}^3$) in Tangshan were
261 significantly lower than the thresholds of the Chinese Ambient Air Quality Standard (CAAQS) (Hg:
262 50 ng/m^3), World Health Organization (WHO) (Hg: 1000 ng/m^3 , Ni: 25 ng/m^3 , and Pb: 1000 ng/m^3),
263 European Union (EU) (Ni: 20 ng/m^3), and the United States (Pb: 150 ng/m^3). However, both of the
264 As ($15 \pm 11 \text{ ng/m}^3$) and Cr concentrations ($2.8 \pm 2.2 \text{ ng/m}^3$) in $\text{PM}_{2.5}$ of Tangshan were much higher
265 than the standard values of the CAAQS (As: 6.0 ng/m^3 and Cr: 0.03 ng/m^3), WHO (As: 6.6 ng/m^3
266 and Cr: 0.25 ng/m^3), and EU (As: 6.0 ng/m^3).

267 The inter-annual variation of the original concentrations of trace elements in $\text{PM}_{2.5}$ are depicted
268 in Figure 3 and S2-S3. The original concentrations of all the trace elements exhibited decreasing
269 trends. Cu, Co, Zn, Pb, As, and Ga concentrations showed dramatic decreases from 37 to 12 ng/m^3
270 (68%), 1.21 to 0.4 ng/m^3 (66%), 400 to 190 ng/m^3 (53%), 71 to 40 ng/m^3 (44%), 20 to 11 ng/m^3
271 (44%), and 1.09 to 0.6 ng/m^3 (42%), respectively. Following these species, the K (40%), Ag (39%),
272 V (39%), Ni (36%), Ca (33%), Mn (29%), Se (29%), Fe (27%), and Cr (21%) concentrations showed
273 moderate decreasing ratios. The observed Hg level exhibited the lowest decreasing ratio from 1.59
274 to 1.43 ng/m^3 (9.9%).

275 3.2 Impact of emission reduction on trace element concentrations

276 Although the original concentrations of the trace elements could be utilized to analyze the impact
277 of the clean air policy, the role of emission reduction on the element concentration might not be
278 clearly clarified because the meteorological factors were also important variables affecting the air
279 quality. In order to accurately reflect the response of the element concentrations to the emission
280 reduction alone during 2017-2020, the meteorological conditions were eliminated by the RF model
281 in our study. Based on the results in Figure S4, the RF models for all of the species showed better
282 performance because their R^2 values were higher than 0.50, and the slopes of all of the fitting curves
283 were also close to the R^2 values. The result suggested that the separation of meteorology and
284 emission of trace elements based on the RF model was reliable. During 2017-2020, the deweathered
285 concentrations of Ga, Co, Pb, Zn, and As showed the rapid decreases from 1.52 to 0.4 ng/m^3 (72%),
286 1.31 to 0.4 ng/m^3 (67%), 92 to 35 ng/m^3 (62%), 410 to 170 ng/m^3 (59%), and 21 to 10 ng/m^3 (54%),

287 respectively (Figure 3). It was well known that As, Co, and Pb were typical marker elements for
288 coal combustion and the “coal-to-gas” and “coal-to-electricity” strategies have been widely
289 performed in Tangshan (Fang et al., 2020; Li et al., 2017). Wang et al. (2020a) have estimated that
290 these effective control measures have contributed to around 60% of the total PM_{2.5} reductions.
291 Meanwhile, the upgradation and optimization of the industrial structure/layout and the shutdown of
292 high-pollution industries were also strictly implemented in Tangshan, and thus led to the dramatic
293 decreases of Ga and Zn concentrations because Ga and Zn were common forms of nonferrous metal
294 smelting (Tian et al., 2015). In contrast, the deweathered Ca level displayed the lowest decrease
295 ratio (8.3%) from 2017 to 2020, indicating that clean air actions cannot significantly reduce the
296 fugitive emissions. In addition, the deweathered Fe (23%) and Cr (18.5%) also suffered from
297 relatively low decrease ratios. It was well documented that Fe and Cr originated from metallurgical
298 industry such as steel production and ferrous metal smelting (Tian et al., 2015), and the slight
299 decreases of the deweathered Fe and Cr levels during the sampling period suggested that the
300 emission control measures for ferrous metal smelting should be strengthened in the future.

301 In addition, the decreasing ratios of the deweathered concentrations for each species displayed
302 different seasonal characteristics. The deweathered concentrations of some elements related with
303 industrial activities (e.g., Ga, Zn, and Cr) showed rapid decreases in autumn and winter compared
304 with other seasons during 2017-2020 (Figure 4), indicating that the optimization of the industrial
305 layout and shutdown of outdated industries were effective to decrease these element emissions
306 especially in the high-pollution season. Some elements derived from biomass burning including K
307 (66%) and Se (50%) also exhibited the most dramatic decreasing ratios in autumn. It was assumed
308 that enhanced crop residual burning occurred frequently during the autumn harvest season. Ke et al.
309 (2019) confirmed that the number of fire spots in October-November was even higher than that in
310 June and the burned area in the harvest season was highest during 2013-2017. However, the control
311 on open biomass burning has been implemented strictly in recent years, largely reducing the K and
312 Se emissions in autumn. It should be noted that the deweathered Pb (46%), Co (65%), and As (45%)
313 concentrations in winter did not display high decreasing ratios though the annual mean deweathered
314 Pb, Co and As levels experienced dramatic decreases. The result revealed that it was still difficult
315 to reduce the Pb, Co, and As emissions during the heating season because increased coal

316 consumption for domestic heating largely offset the contributions of emission control measures
317 (Zhu et al., 2018; Zhu et al., 2020).

318 Apart from the seasonal difference of each species, the decreasing ratios of these elements also
319 suffered from distinctly intra-weekly variations. The deweathered concentrations of most elements
320 except Ca, Cu, Ni, and V exhibited higher decreasing ratios at the weekends than on the weekdays
321 (Figure 5). Cui et al. (2020) have demonstrated that the weaker supervision on industrial enterprises
322 on weekends could lead to the higher concentrations of non-traffic elements such as K, As, Se, and
323 Cr in some cities. Fortunately, grid monitoring has been widely performed in Tangshan recently
324 (<http://hbepb.hebei.gov.cn/hbhjt/xwzx/jicengfengcai/101624062321621.html>), and many low-cost
325 sensors were installed at some energy-intensive industries, which could decrease the stealing
326 emissions of some elements. Nonetheless, the decreasing ratios of Ca, Cu, V, and Ni did not show
327 the regular intra-weekly characteristics. In recent years, Tangshan adopted strict traffic management
328 regulation and the nonlocal light duty vehicles were restricted to drive inside the urban area one day
329 per week based on the end number of the license plates (Westerdahl et al., 2009; Wu et al., 2011),
330 whereas the restrictions were not valid at weekends (Liu et al., 2007). Theoretically, the traffic
331 control should result in marked decreases of traffic-related element concentrations on weekdays
332 compared with weekends. However, in our study, some traffic-related elements such as Ca and Cu
333 did not show similar characteristics. Meanwhile, as the important tracer of vehicle emission, the
334 NO_x concentration in Tangshan did not show a regular intra-weekly pattern. It was supposed that
335 the vehicle volume in Tangshan has increased from 2.0 to 2.4 million (<http://tjj.hebei.gov.cn/>),
336 which largely offset the benefits of traffic controls. The shipping-related elements including V and
337 Ni also did not show regular intra-weekly variation because no heavy metal emission control
338 measures for shipping were performed.

339 3.3 The role of meteorology on the year-to-year variations of element concentrations

340 The difference between the original and deweathered element concentrations could be regarded
341 as the concentrations contributed by meteorological parameters. The positive impacts of
342 meteorological parameters on the trace elements suggested that the meteorological conditions were
343 unfavorable to the pollutant diffusion, while the negative impacts of meteorological indicators
344 meant the favorable condition to trace elements. In our study, the roles of meteorological conditions

345 on Ca (-25%), V (-10%), Cr (-2.5%), Mn (-0.7%), Fe (-4.6%), Ni (-7.6%), and Cu (-21%) during
346 2017-2020 were negative (Figure S5), while the roles of meteorological parameters on other
347 elements were positive. The result suggested that those elements derived from vehicle emission (Ca,
348 Cu, and Fe), ferrous metal smelting (Cr and Mn), and heavy oil combustion (V and Ni) were less
349 sensitive to the emission reduction actions compared with other elements and the meteorological
350 conditions were much beneficial to the diffusion of these elements. In order to further reveal the key
351 meteorological factors for these elements, we used the RF model to calculate the variable
352 importance of all of these meteorological parameters including P, RH, T, WD, and WS. The result
353 suggested that Ca, Fe, and Cu were mainly influenced by T, whereas V, Ni, Cr, and Mn were often
354 associated with WD and WS (Figure 6). During the spring and summer in 2017-2020, the average
355 air temperature decreased from 8.9 and 27 to 7.2 and 26°C, respectively. The decreased air
356 temperature led to a higher water content in the soil and a lower tendency of dust suspension, and
357 might decrease the concentrations of Ca, Fe, and Cu (Manju et al., 2018; Yang et al., 2017; Lyu et
358 al., 2016). Although the annual average wind speed in Tangshan decreased from 1.70 to 1.45 m/s,
359 the mean wind speed from the southeastern direction displayed a slight increase from 1.34 to 1.50
360 m/s. Zhao et al. (2013) verified that V and Ni were usually emitted from heavy oil combustion of
361 ocean-going ship engines. Many coastal ports and ferrous metal smelting industries were located on
362 the southeastern direction of the sampling site, and thus the enhanced WS might promote the
363 dilution and dispersion of trace elements (Figures S6-S8). As shown in Figure S8, both of V and Ni
364 showed the higher concentrations in the southeastern part of Tangshan and the concentrations
365 displayed gradual decreases along the Southeast-Northwest transect, which also demonstrated that
366 both of V and Ni in the sampling site could be derived from coastal shipping emission.

367 3.4 The impact of clean air policy on the source apportionment of trace elements

368 Although the major sources of elements could be determined based on some important tracers
369 (e.g., K, V), the contributions of the major sources to each element still remained unknown.
370 Therefore, Positive matrix factorization (version PMF 5.0) was applied to identify more source
371 information of the elements in PM_{2.5} during 2017-2020 based on the deweathered levels. After 20
372 runs, more than 26000 samples were trained to determine the optimal six factors with the lowest
373 values of Q (robust) and Q (true). The BS, DISP, and BS-DISP methods confirmed that the most

374 reliable solution was obtained with six factors. The detailed information of the PMF analysis and
375 error diagnostics is summarized in Table S4-S6.

376 As shown in Figure S9, the trace elements in PM_{2.5} during 2017-2020 showed similar
377 characteristics. Factor 1 possesses high loadings of K (55%) and Se (42%). K and Se were often
378 regarded as the major tracers of biomass burning. Due to the increasing usage of biomass fuels for
379 domestic heating during the heating season, K and Se in PM_{2.5} of Tangshan showed higher values
380 in winter, suggesting that these metals in fine particles could originate from the combustion of
381 biomass fuels. Except for the domestic heating, we found some episodes during the harvesting
382 season in late summer (2500 and 11.2 ng/m³) and early autumn (2600 and 9.5 ng/m³) also showed
383 extremely high concentrations of K, which might be linked with local biomass burning (Chen et al.,
384 2017). Based on the map of fire points and backward air masses trajectories (Figures S6-S8), the
385 metals released from biomass burning in the NCP could be transported to the sampling site by the
386 dominant southerly wind, which further proved the impacts of biomass burning (Chen et al., 2017).

387 The abundant elements in factor 2 included Ag (53%), Zn (51%), and Cu (36%). Owing to the
388 higher temperatures during the roasting, sintering and smelting processes for the extraction of Cu,
389 and Zn from ores, some metals such as Ag in nonferrous metal ores could be vaporized as a
390 byproduct and released into the flue gas (Pacyna and Pacyna, 2001; Wu et al., 2012). Therefore,
391 factor 2 was interpreted as the non-ferrous metal smelting source.

392 Factor 3 was characterized by a large mass fraction of Co (81%), Pb (61%), Hg (57%), and As
393 (39%). After the phase-out of leaded gasoline since 1980s, the contribution from coal combustion
394 to Pb showed rapid increase and accounted for the major fraction of particulate Pb (Das et al., 2018).
395 Meanwhile, Co and Hg were also treated as important byproducts released from coal burning and
396 the Co and Hg concentrations often increased significantly with the elevation of the burning
397 temperature (Tang et al., 2018). Tian et al. (2015) estimated that 73% of As, 56 % of Pb, and 47 %
398 of Hg were found to be emitted from coal combustion in China. Coal consumption in South China
399 was mainly driven by coal-fired power plants, while the coal-based heating was the major sector for
400 the coal consumption in the NCP. In our study, As, Co and Pb showed the higher concentrations in
401 winter (heating season) (18.7, 0.9, and 76 ng/m³) compared with other seasons (14, 0.6, and 51
402 ng/m³). The markedly seasonal discrepancies of As, Co and Pb strongly supported the impact of the

403 coal combustion for domestic heating on the enhancement of As, Co and Pb in the fine particles.

404 Factor 4 was distinguished by high loadings of Cr (78%) and Mn (39%), respectively. Cr and
405 Mn mainly originated from metallurgical industry such as steel production and ferrous metal
406 smelting (Liu et al., 2018a; Tian et al., 2015; Zhu et al., 2018). China was responsible for more than
407 49% of the world steel production in 2017 (approximate 830 million tons), and 60% of the large
408 steel producers were located in China (Chang et al., 2018). Tangshan possesses many large steel
409 production industries such as Tangshan Steel, Qian'an Steel, and Guofeng Steel. Besides, some
410 industries of Capital Steel have been migrated into Tangshan (Li et al., 2019), which might increase
411 the Cr and Mn emissions.

412 Factor 5 explained 10.1% of the total species and it was characterized by high loadings of V
413 (88%) and Ni (51%). It was well documented that V was a key fingerprint of heavy oil combustion,
414 which was generally emitted from shipping emission and petrochemical refining (Shafer et al.,
415 2012). Ni was widely utilized as a tracer of fuel oil combustion in industries (Zhu et al., 2018).
416 Many oil-fired power plants were located in Tangshan for central heating (Yu et al., 2013). Based
417 on the backward trajectory and wind direction (Figures S6-S8), we found that high concentrations
418 of V and Ni might be derived from the southeastern air masses especially in summer and autumn,
419 indicating the impacts of coastal port and petroleum refinery industry. In addition, the V and Ni
420 concentrations displayed the gradual decreases along the Southeast-Northwest transect, indicating
421 the potential sources were located on Southeast Tangshan (Figure S8). Gathering evidence
422 suggested that the V/Ni ratio in petroleum coke with a low-sulfur content and fuel oil usage ranged
423 from 1 to 3 (Moreno et al., 2010). The annual mean ratios of V and Ni in our study reached 1.2
424 during the sampling period, which was in the range of this interval. The result also revealed that
425 petrochemical refining and heavy oil combustion derived from coastal shipping emission might be
426 an important source of V and Ni in the fine particles.

427 Factor 6 was characterized by high loadings of Ca (78%), Cu (32%), and Fe (33%), and moderate
428 loadings of Mn (31%) and Zn (29%). Some previous studies have demonstrated that Cu, Fe, and Zn
429 were released from tyre and brake wear because they were the necessary materials for brake pads
430 and the agents in brake linings (Dall'Osto et al., 2013; Hjortenkrans et al., 2007). Ca probably
431 originated from the road fugitive dust because it was one of the most abundant elements in the upper

432 soil (Alves et al., 2015; Liu et al., 2018a). Moreover, we have found Fe, Ca, and Zn displayed
433 remarkably high values during the morning rush hours and a small peak during the sunset (Figure
434 S10), which was coincident to the diurnal variation of the traffic volume. Thus, the factor 6 was
435 identified as the traffic-related dust source.

436 Although six similar sources were revealed during 2017-2020, the contribution concentrations
437 and ratios of these sources varied greatly in these years. As shown in Figures 7 and 8, the
438 contribution concentrations of biomass burning, non-ferrous metal smelting, coal combustion, and
439 ferrous metal smelting to trace elements decreased from 1460, 480, 640, and 570 ng/m³ to 900, 230,
440 230, and 350 ng/m³, respectively. However, the contribution concentrations of heavy oil combustion
441 and traffic-related dust displayed a slight increase during 2017-2019, while they decreased rapidly
442 after 2019. The contribution concentrations for nearly all sources to trace elements suffered from
443 decreases during 2017-2020 because the total deweathered levels of trace elements experienced
444 decreases in the past three years. However, the contribution ratios of these sources to the trace
445 elements did not show similar characteristics. For instance, the contribution ratio of the traffic-
446 related dust increased from 25% to 33%. In contrast, the contributions of non-ferrous metal smelting
447 and coal combustion decreased from 11% to 8% and 15% to 8%, respectively. The contributions of
448 ferrous metal smelting, heavy oil combustion, and biomass burning remained relatively stable
449 during this period.

450 Due to the strict implementation of the clean air policy, many outdated industrial capacities were
451 shut down and cleaner technologies have been upgraded, which facilitated the production decreases
452 of pig iron and coal-fired power plants (Ma et al., 2019). Hence, the contribution concentrations and
453 ratios of non-ferrous metal smelting and coal combustion experienced dramatic decreases. Although
454 the open biomass burning has been strictly restricted in Tangshan (Chang et al., 2018), the
455 contribution ratios of biomass burning to the trace elements in PM_{2.5} remained relatively stable,
456 which might be attributable to the rapid decreases of the contributions derived from coal combustion
457 and non-ferrous metal smelting. In addition, the biofuel combustion was still widespread in some
458 rural and suburb areas (Kamal et al., 2015; Li et al., 2020), which might offset the decreases in the
459 contributions of open biomass burning. Although the contribution concentrations of traffic-related
460 dust to trace elements also showed slight decrease, the contribution ratios of traffic-related dust to

461 some trace elements exhibited marked increases (8%) during 2017-2020 because the contribution
462 ratios of metal smelting and coal combustion displayed substantial decreases. The result also
463 demonstrated that the implementation of coal to gas project facilitated the decreases of trace element
464 concentrations. In addition, the source variation trend also suggested that the formulation of many
465 new quality standards for non-road diesel fuels cannot fully decrease the element emissions (Cui et
466 al., 2017), and thus the control of traffic-related dust should be enhanced in the future.

467 3.5 Health risk assessment of trace metals in PM_{2.5}

468 Although the trace metals only accounted for a minor fraction of the total mass concentration of
469 PM_{2.5}, it might pose a great threat to the human health because most of these metals were
470 bioavailable and non-degradable (Rai et al., 2019; Yi et al., 2011). Unfortunately, previous studies
471 mainly used filter sampling techniques to determine the concentrations of trace metals and then
472 assess their health risks (Cui et al., 2018; Huang et al., 2016). These low-resolution data might not
473 accurately reflect the real health risks triggered by metal exposure. In our study, we employed online
474 data to assess the health risks derived from metal exposure.

475 The health risks of trace metals could be classified into two types including carcinogenic and
476 non-carcinogenic risk. Based on the major parameters summarized in Tables S7 and S8, we
477 estimated both of the carcinogenic and non-carcinogenic risks of the major metals. To evaluate the
478 impacts of emission control measures on the element concentrations, both the health risks based on
479 original element levels and the deweathered element concentrations were calculated. The mean CR
480 values based on the original concentrations were in the order of Pb (2.3×10^{-6} (adult) and 1.4×10^{-6}
481 (child)) > As (1.9×10^{-6} and 1.1×10^{-6}) > Cr (0.11×10^{-6} and 0.07×10^{-6}). The total CR values for adults
482 and children reached 4.3×10^{-6} and 2.6×10^{-6} (Table 2), respectively. The total CR values were located
483 in the range of the acceptable (10^{-6}) and least stringent risk levels (10^{-4}), which suggested that
484 Tangshan suffered from a slight metal carcinogenic risk. Among all of these metals, Pb and As
485 displayed the higher CR values. It was assumed that the coal combustion for domestic heating might
486 be the dominant factor for the higher risks of Pb and As in Tangshan because both Pb and As in
487 PM_{2.5} were mainly derived from coal combustion. With regard to the non-carcinogenic risks of the
488 trace metals, the HQ of As (1.2×10^{-2} and 2.9×10^{-2}) and Pb (6.8×10^{-4} and 17×10^{-4}) showed higher
489 values compared with other elements. The result indicated that nearly all elements did not display

490 potential non-carcinogenic risk because the HQ values of all the metals were less than 1. The total
491 HQ value of these metals was also lower than 1, indicating that the trace elements in Tangshan did
492 not show a significant non-carcinogenic risk.

493 By removing the impact of the meteorological conditions, we can isolate the impact of the clean
494 air policy on health risks associated with metal exposure alone. The decrease ratios of the CR values
495 based on the deweathered As and Pb concentrations during 2017-2020 were 54% and 62%,
496 respectively (Table 3). However, the decrease ratios of the CR values based on the original As and
497 Pb levels only reached 44%. The result suggested that the clean air policy in recent years
498 significantly decreased the As and Pb emissions. Additionally, the decrease ratios of HQ values for
499 the original Cu (41%) and Zn (53%) were much less than those for the deweathered ones (Cu: 47%
500 and Zn: 59%). Nevertheless, some other elements did not show similar characteristics. For instance,
501 the decreased ratios of the HQ values for the original Cr (21%) and Fe (27%) were even slightly
502 higher than those for the deweathered ones (Cr: 19% and Fe: 23%). It was assumed that the clean
503 air policy in recent years facilitated the emission reduction of non-ferrous metal smelting and coal
504 combustion efficiently. However, the concentrations of the elements derived from ferrous metal
505 smelting and vehicle emission did not show marked decreases, which was in good agreement with
506 the source apportionment result in section 3.3. Thus, in the future work, it is highly imperative to
507 further reduce the industrial/traffic-related emissions in order to alleviate potential health risks.

508 3.6 Limitations and uncertainties

509 It should be noted that our work is still subject to some limitations. At first, some elements such as
510 Cr (0.5) and Ga (0.5) showed relatively lower CV R² values though they were generally higher than
511 0.5. These elements might show the higher uncertainties during the meteorology-normalization
512 compared with other elements such as Cu (0.85) and K (0.85). Besides, few variables were applied
513 to deweather the element concentrations, which might be responsible for the lower CV R² value for
514 some elements. Due to the lack of available hourly emission inventory of each element, we only
515 used the time variable to train the model. This method still suffered from some uncertainties, which
516 should be improved by the establishment of near-time emission database.

517 4. Conclusions and implications

518 Three-year continuous hourly observation of elements in PM_{2.5} was conducted in Tangshan

519 during September 2017-August 2020. The effect of the clean air policy on the element
520 concentrations in PM_{2.5} was quantified. The main conclusions were drawn as follows:

521 (1) The deweathered concentrations of Ga, Co, Pb, Zn, and As showed rapid decreases from 1.52
522 to 0.42 ng/m³ (72%), 1.31 to 0.44 ng/m³ (67%), 92 to 35 ng/m³ (62%), 411 to 170 ng/m³ (59%),
523 and 21 to 10 ng/m³ (54%), respectively. The clean air actions played the important role on the
524 emission reduction of coal combustion and non-ferrous metal smelting.

525 (2) The deweathered levels of Ca (8.3%), Cr (19%), and Fe (23%) displayed relatively low
526 decreases compared with other elements, indicating that the vehicle emission and ferrous-
527 smelting industries might not be sensitive to the air clean policy.

528 (3) The deweathered levels of some elements related with industrial activities (e.g., Ga, Zn, and Cr)
529 exhibited rapid decreases in autumn and winter compared with other seasons during 2017-2020,
530 while the combustion-related elements such as Pb and As did not show high decreasing ratios
531 in winter. The enhanced coal consumption during the heating season offsets the benefits derived
532 from strict emission control measures.

533 (4) The favorable meteorological conditions promoted the decreases of Ca (-25%), V (-10%), Cr (-
534 2.6%), Mn (-0.68%), Fe (-4.6%), Ni (-7.6%), and Cu (-21%) concentrations.

535 (5) The contribution ratios of biomass burning, non-ferrous metal smelting, coal combustion,
536 ferrous metal smelting, heavy oil combustion, and traffic-related dust changed from 33%, 11%,
537 15%, 13%, 3%, and 25% to 33%, 8%, 8%, 13%, 4%, and 33%, respectively.

538 (6) All elements did not show significant noncarcinogenic and carcinogenic risks, while both As
539 and Pb still displayed relatively high health damages.

540 Our study presented detailed information about the impact of clean air policy on the chemical
541 compositions and source apportionment of trace elements in PM_{2.5} in Tangshan, and provided new
542 insights for the scientific community and policymakers. Many targeted measures could be
543 undertaken to alleviate the air pollution and further to reduce avoided premature health risks.
544 However, this study still suffered some limitations and more steps will be taken toward thoroughly
545 addressing these problems. First of all, the PMF model still showed some uncertainties, and thus
546 characterizing the isotopic signatures of the elements is of great significance. In addition, a Sunset
547 OC/EC analyzer, a Monitoring of Aerosols and Gases (MARGA) platform, and other on-line

548 measurements should be collocated to probe into the synergistic effect of emission reduction and
549 meteorology on air quality.

550 **Acknowledgements**

551 This work was supported by the National Natural Science Foundation of China (42107113).

552 **Data availability**

553 The boundary layer height dataset was obtained from the website of <https://www.ecmwf.int/>. The
554 dataset is archived in <https://zenodo.org/record/7031975#.Ywys8cjfmfU> (Li et al., 2022).

555 **Author contributions**

556 LR wrote the manuscript. LR, PM, ZWD, and HJM contributed to the conceptualization of the study.

557 LR and PM conducted the research, and visualized the results. WGH revised the manuscript.

558 **Competing interests**

559 The contact authors have declared that neither they nor their co-authors have any competing
560 interests.

561 **References**

- 562 Alies, B., Sasaki, I., Proux, O., Sayen, S., Guillon, E., Faller, P., and Hureau, C.: Zn impacts Cu
563 coordination to amyloid- β , the Alzheimer's peptide, but not the ROS production and the associated
564 cell toxicity, *Chem. Commun.*, 49, 1214-1216, 2013.
- 565 Alves, C., Gomes, J., Nunes, T., Duarte, M., Calvo, A.I., Custodio, D., Pio, C., Karanasiou, A., and
566 Querol, X.: Size-segregated particulate matter and gaseous emissions from motor vehicles in a road
567 tunnel, *Atmos. Res.*, 153, 134-144, <https://doi.org/10.1016/j.atmosres.2014.08.002>, 2015.
- 568 Ao, M., Qiu, G., Zhang, C., Xu, X., Zhao, L., Feng, X., Qin, S., and Meng, B.: Atmospheric deposition
569 of antimony in a typical mercury-antimony mining area, Shaanxi Province, Southwest China, *Environ.*
570 *Pollut.*, 245, 173-182, <https://doi.org/10.1016/j.envpol.2018.10.125>, 2019.
- 571 Chang, Y., Huang, K., Xie, M., Deng, C., Zou, Z., Liu, S., and Zhang, Y.: First long-term and near real-
572 time measurement of trace elements in China's urban atmosphere: temporal variability, source
573 apportionment and precipitation effect, *Atmos. Chem. Phys.*, 18, 11793-11812,
574 <https://doi.org/10.5194/acp-18-11793-2018>, 2018.
- 575 Chen, J., Li, C., Ristovski, Z., Milic, A., Gu, Y., Islam, M.S., Wang, S., Hao, J., Zhang, H., and He, C.: A
576 review of biomass burning: Emissions and impacts on air quality, health and climate in China, *Sci.*
577 *Total Environ.*, 579, 1000-1034, <https://doi.org/10.1016/j.scitotenv.2016.11.025>, 2017.
- 578 Chen, G.B., Li, S.S., Knibbs, L.D., Hamm, N.A.S., Cao, W., Li, T.T., Guo, J.P., Ren, H.Y., Abramson,
579 M.J., and Guo, Y.M.: A machine learning method to estimate PM_{2.5} concentrations across China with
580 remote sensing, meteorological and land use information, *Sci. Total Environ.*, 636, 52-60,
581 <https://doi.org/10.1016/j.scitotenv.2018.04.251>, 2018.
- 582 Clements, A.L., Buzcuguvan, B., Fraser, M.P., Kulkarni, P., and Chellam, S.: Role of particulate metals
583 in heterogenous secondary sulfate formation, *Atmos. Environ.*, 75, 233-240,
584 <https://doi.org/10.1016/j.atmosenv.2013.04.038>, 2013.
- 585 Clements, N., Eav, J., Xie, M., Hannigan, M. P., Miller, S. L., Navidi, W., et al.: Concentrations and
586 source insights for trace elements in fine and coarse particulate matter, *Atmos. Environ.*, 89, 373-381,
587 <https://doi.org/10.1016/j.atmosenv.2014.01.011>, 2014.
- 588 Cui, L., Duo, B., Zhang, F., Li, C., Fu, H., and Chen, J.: Physiochemical characteristics of aerosol
589 particles collected from the Jokhang Temple indoors and the implication to human exposure, *Environ.*
590 *Pollut.*, 236, 992-1003, <https://doi.org/10.1016/j.envpol.2017.10.107>, 2018.
- 591 Cui, M., Chen, Y., Feng, Y., Li, C., Zheng, J., Tian, C., Yan, C., and Zheng, M.: Measurement of PM and
592 its chemical composition in real-world emissions from non-road and on-road diesel vehicles, *Atmos.*
593 *Chem. Phys.*, 17, 6779-6795, <https://doi.org/10.5194/acp-17-6779-2017>, 2017.
- 594 Cui, X., Wang, X., and Liu, B.: The characteristics of heavy metal pollution in surface dust in Tangshan,
595 a heavily industrialized city in North China, and an assessment of associated health risks, *J. Geochem.*
596 *Explor.*, 210, 106432, 2020.
- 597 Cui, Y., Ji, D., Chen, H., Gao, M., Maenhaut, W., He, J., and Wang, Y.: Characteristics and sources of
598 hourly trace elements in airborne fine particles in urban Beijing, China, *J. Geophys. Res. Atmos.*, 124,
599 11595-11613, <https://doi.org/10.1029/2019JD030881>, 2019.
- 600 D'Alessandro, A., Lucarelli, F., Mandò, P.A., Marcazzan, G., Nava, S., Prati, P., Valli, G., Vecchi, R.,
601 Zucchiatti, A.: Hourly elemental composition and sources identification of fine and coarse PM₁₀
602 particulate matter in four Italian towns, *J. Aerosol Sci.*, 34, 243-259, 2003.
- 603

604 Dall'Osto, M., Querol, X., Amato, F., Karanasiou, A., Lucarelli, F., Nava, S., Calzolari, G., and Chiari,
605 M.: Hourly elemental concentrations in PM_{2.5} aerosols sampled simultaneously at urban background
606 and road site during SAPUSS -diurnal variations and PMF receptor modelling, *Atmos. Chem. Phys.*,
607 13, 4375-4392, 2013.

608 Das, R., Mohtar, A.T.B.M., Rakshit, D., Shome, D., and Wang, X.: Sources of atmospheric lead (Pb) in
609 and around an Indian megacity, *Atmos. Environ.*, 193, 57-65,
610 <https://doi.org/10.1016/j.atmosenv.2018.08.062>, 2018.

611 Duan, J. and Tan, J.: Atmospheric heavy metals and arsenic in China: situation, sources and control
612 policies, *Atmos. Environ.*, 74, 93-101, [10.1016/j.atmosenv.2013.03.031](https://doi.org/10.1016/j.atmosenv.2013.03.031), 2013.

613 Fang, B., Zhang, L., Zeng, H., Liu, J., Yang, Z., Wang, H., Wang, Q., and Wang, M.: PM_{2.5}-bound
614 polycyclic aromatic hydrocarbons: sources and health risk during non-heating and heating periods
615 (Tangshan, China), *Int. J. Env. Res. Pub. He.*, 17, 483, 2020.

616 Fernandez, J.A., Rey, A., and Carballeira, A.: An extended study of heavy metal deposition in Galicia
617 (NW Spain) based on moss analysis, *Sci. Total Environ.*, 254, 31-44, [10.1016/s0048-9697\(00\)00431-](https://doi.org/10.1016/s0048-9697(00)00431-9)
618 9, 2000.

619 Furger, M., Minguillon, M.C., Yadav, V., Slowik, J.G., Hüglin, C., Frohlich, R., Petterson, K.,
620 Baltensperger, U., and Prevot, A.S.H.: Elemental composition of ambient aerosols measured with high
621 temporal resolution using an online XRF spectrometer, *Atmos. Meas. Tech.*, 10, 2061-2076,
622 <https://doi.org/10.5194/amt-10-2061-2017>, 2017.

623 Geng, G., Xiao, Q., Zheng, Y., Tong, D., Zhang, Y., Zhang, X., Zhang, Q., He, K., and Liu, Y.: Impact of
624 China's air pollution prevention and control action plan on PM_{2.5} chemical composition over eastern
625 China, *Sci. China Earth Sci.*, 62, 1872-1884, <https://doi.org/10.1007/s11430-018-9353-x>, 2019.

626 Grivas, G., Cheristanidis, S., Chaloulakou, A., Koutrakis, P., & Mihalopoulos, N.: Elemental composition
627 and source apportionment of fine and coarse particles at traffic and urban background locations in
628 Athens, Greece, *Aerosol Air Qual. Res.*, 18, 1642-1659, 2018.

629 Guo, J., Tilgner, A., Yeung, C., Wang, Z., Louie, P.K.K., Luk, C.W.Y., Xu, Z., Yuan, C., Gao, Y., and
630 Poon, S.: Atmospheric peroxides in a polluted subtropical environment: seasonal variation, sources
631 and sinks, and importance of heterogeneous processes, *Environ. Sci. Technol.*, 48, 1443-1450,
632 <https://doi.org/10.1021/es403229x>, 2014.

633 Harmens, H., Norris, D.A., Steinnes, E., Kubin, E., Piispanen, J., Alber, R., Aleksiyenak, Y., Blum, O.,
634 Coskun, M., and Dam, M.: Mosses as biomonitors of atmospheric heavy metal deposition: Spatial
635 patterns and temporal trends in Europe, *Environ. Pollut.*, 158, 3144-3156,
636 <https://doi.org/10.1016/j.envpol.2010.06.039>, 2010.

637 He, Q., Zhang, M., Song, Y., and Huang, B.: Spatiotemporal assessment of PM_{2.5} concentrations and
638 exposure in China from 2013 to 2017 using satellite-derived data, *J. Cleaner Prod.*, 286, 124965,
639 <https://doi.org/10.1016/j.jclepro.2020.124965>, 2021.

640 Hjortenkrans, D.S., Bergbäck, B.G., and Häggerud, A.V.: Metal emissions from brake linings and tires:
641 case studies of Stockholm, Sweden 1995/1998 and 2005, *Environ. Sci. Technol.*, 41, 5224-5230,
642 <https://doi.org/10.1021/es070198o>, 2007.

643 Holden, P.A., Gardeatorresdey, J.L., Klaessig, F., Turco, R.F., Mortimer, M., Hundrinke, K., Hubal,
644 E.A.C., Avery, D., Barcelo, D., and Behra, R.: Considerations of environmentally relevant test
645 conditions for improved evaluation of ecological hazards of engineered nanomaterials, *Environ. Sci.*
646 *Technol.*, 50, 6124-6145, <https://doi.org/10.1021/acs.est.6b00608>, 2016.

647 Huang, C., Bao, L., Luo, P., Wang, Z., Li, S., and Zeng, E.Y.: Potential health risk for residents around a

648 typical e-waste recycling zone via inhalation of size-fractionated particle-bound heavy metals, J.
649 Hazard. Mater., 317, 449-456, 10.1016/j.jhazmat.2016.05.081, 2016.

650 Jeong, C., Wang, J.M., and Evans, G.J.: Source apportionment of urban particulate matter using hourly
651 resolved trace metals, organics, and inorganic aerosol components, Atmos. Chem. Phys., 1-32,
652 <https://doi.org/10.5194/acp-2016-189>, 2016.

653 Kamal, A., Cincinelli, A., Martellini, T., and Malik, R.N.: A review of PAH exposure from the combustion
654 of biomass fuel and their less surveyed effect on the blood parameters, Environ. Sci. Pollut. Res., 22,
655 4076-4098, 10.1007/s11356-014-3748-0, 2015.

656 Kang, S., Chen, P., Li, C., Liu, B., and Cong, Z.: Atmospheric aerosol elements over the inland Tibetan
657 Plateau: concentration, seasonality, and transport, Aerosol Air Qual. Res., 16, 789-800, 2016.

658 Ke, H.B., Gong, S.L., He, J.J., Zhou, C.H., Zhang, L., Zhou, Y.K.: Spatial and temporal distribution of
659 open bio-mass burning in China from 2013 to 2017, Atmos. Environ., 210, 156-165, 2019.

660 Li, R., Fu, H., Cui, L., Li, J., Wu, Y., Meng, Y., Wang, Y., and Chen, J.: The spatiotemporal variation and
661 key factors of SO₂ in 336 cities across China, J. Cleaner Prod., 210, 602-611,
662 <https://doi.org/10.1016/j.jclepro.2018.11.062>, 2019.

663 Li, R., Zhao, Y., Fu, H., Chen, J., Peng, M., and Wang, C.: Substantial changes in gaseous pollutants and
664 chemical compositions in fine particles in the North China Plain during the COVID-19 lockdown
665 period: anthropogenic vs. meteorological influences, Atmos. Chem. Phys., 21, 8677-8692,
666 <https://doi.org/10.5194/acp-21-8677-2021>, 2021.

667 Li, R., Peng, M., Zhao, W.D., Wang, G.H., and Hao, J.M.: Data for “Measurement Report: Rapid changes
668 of chemical characteristics and health risks for high time-resolved trace elements in PM_{2.5} in a typical
669 industrial city in response to stringent clean air actions”, [dataset],
670 <https://zenodo.org/record/7031975#.Ywys8cjfmfU>, 2022.

671 Li, Z., Jiang, J., Ma, Z., Fajardo, O.A., Deng, J., and Duan, L.: Influence of flue gas desulfurization (FGD)
672 installations on emission characteristics of PM_{2.5} from coal-fired power plants equipped with selective
673 catalytic reduction (SCR), Environ. Pollut., 230, 655-662,
674 <https://doi.org/10.1016/j.envpol.2017.06.103>, 2017.

675 Li, Z., Wang, Y., Li, Z., Guo, S., and Hu, Y.: Levels and sources of PM_{2.5}-associated pahs during and after
676 the wheat harvest in a central rural area of the beijing-tianjin-hebei (bth) region, Aerosol Air Qual.
677 Res., 20, 1070-1082, 2020.

678 Lin, Y., Hsu, S., Chou, C.C.K., Zhang, R., Wu, Y., Kao, S., Luo, L., Huang, C., Lin, S., and Huang, Y.:
679 Wintertime haze deterioration in Beijing by industrial pollution deduced from trace metal fingerprints
680 and enhanced health risk by heavy metals, Environ. Pollut., 208, 284-293,
681 <https://doi.org/10.1016/j.envpol.2015.07.044>, 2016.

682 Liu, H., He, K., Wang, Q., Huo, H., Lents, J., Davis, N., Nikkila, N., Chen, C., Osses, M., and He, C.:
683 Comparison of vehicle activity and emission inventory between Beijing and Shanghai, J. Air Waste
684 Manage., 57, 1172-1177, <https://doi.org/10.3155/1047-3289.57.10.1172>, 2007.

685 Liu, J., Chen, Y., Chao, S., Cao, H., Zhang, A., and Yang, Y.: Emission control priority of PM_{2.5}-bound
686 heavy metals in different seasons: A comprehensive analysis from health risk perspective, Sci. Total
687 Environ., 644, 20-30, <https://doi.org/10.1016/j.scitotenv.2018.06.226>, 2018a.

688 Liu, R., Men, C., Yu, W., Xu, F., Wang, Q., and Shen, Z.: Uncertainty in positive matrix factorization
689 solutions for PAHs in surface sediments of the Yangtze River Estuary in different seasons,
690 Chemosphere, 191, 922-936, <https://doi.org/10.1016/j.chemosphere.2017.10.070>, 2018b.

691 Lopez-Cruz, J., Crespo-Salvador, O., Fernandez-Crespo, E., Garcia-Agustin, P., and Gonzalez-Bosch, C.:

692 Absence of Cu-Zn-superoxide dismutase BCSOD1 reduces *Botrytis cinerea* virulence in *Arabidopsis*
693 and in tomato plants, which reveals interplay among ROS, callose and signaling pathways, *Mol. Plant*
694 *Pathol.*, 18, 16-31, 2016.

695 Lyu, X.P., Chen, N., Guo, H., Zeng, L.W., Zhang, W.H., Shen, F., Quan, J.H., Wang, N.: Chemical
696 characteristics and causes of airborne particulate pollution in warm seasons in Wuhan, central China,
697 *Atmos. Chem. Phys.*, 16, 10671-10687, www.atmos-chem-phys.net/16/10671/2016/, 2016

698 Lyu, Y., Zhang, K., Chai, F., Cheng, T., Yang, Q., Zheng, Z., and Li, X.: Atmospheric size-resolved trace
699 elements in a city affected by non-ferrous metal smelting: Indications of respiratory deposition and
700 health risk, *Environ. Pollut.*, 224, 559-571, <https://doi.org/10.1016/j.envpol.2017.02.039>, 2017.

701 Ma, Z., Liu, R., Liu, Y., and Bi, J.: Effects of air pollution control policies on PM_{2.5} pollution
702 improvement in China from 2005 to 2017: a satellite-based perspective, *Atmos. Chem. Phys.*, 19,
703 6861-6877, <https://doi.org/10.5194/acp-19-6861-2019>, 2019.

704 Manju, A., Kalaiselvi, K., Dhananjayan, V., Palanivel, M., Banupriya, G., Vidhya, M., Panjakumar, K.,
705 and Ravichandran, B.: Spatio-seasonal variation in ambient air pollutants and influence of
706 meteorological factors in Coimbatore, southern India, *Air Qual. Atmos. Heal.*, 11, 1179-1189,
707 <https://doi.org/10.1007/s11869-018-0617-x>, 2018.

708 Manousakas, M., Papaefthymiou, H., Diapouli, E., Migliori, A., Karydas, A.G., Bogdanovic-Radovic, I.,
709 and Eleftheriadis, K.: Assessment of PM_{2.5} sources and their corresponding level of uncertainty in a
710 coastal urban area using EPA PMF 5.0 enhanced diagnostics, *Sci. Total Environ.*, 574, 155-164, 2017.

711 Micheline, G., Rachida, C., Celine, M., Gaby, K., Rachid, A., and Petru, J.: Levels of Pb, Cd, Hg and As
712 in fishery products from the eastern Mediterranean and human health risk assessment due to their
713 Consumption, *Interna. J. Environ. Res.*, 13, 443-455, <https://doi.org/10.1007/s41742-019-00185-w>,
714 2019.

715 Moreno, T., Querol, X., Alastuey, A., La Rosa, J.D.D., La Campa, A.M.S.D., Minguillon, M., Pandolfi,
716 M., Gonzalez-Castanedo, Y., Monfort, E., and Gibbons, W.: Variations in vanadium, nickel and
717 lanthanoid element concentrations in urban air, *Sci. Total Environ.*, 408, 4569-4579,
718 <https://doi.org/10.1016/j.scitotenv.2010.06.016>, 2010.

719 Norris, G., Duvall, R., Brown, S., and Bai, S.: EPA positive matrix factorization (PMF) 5.0 fundamentals
720 and user guide. U.S, Environmental Protection Agency Office of Research and Development,
721 Washington, DC, 20460, (i-124, EPA/600/R-14/108, April), 2014.

722 Oldani, K.M., Mladenov, N., Williams, M., Campbell, C.M., and Lipson, D.A.: Seasonal patterns of dry deposition at a high-
723 elevation site in the Colorado rocky mountains, *J. Geophys. Res. Atmos.*, 122, 11183-11200, 2017.

724 Olujimi, O.O., Oputu, O., Fatoki, O.S., Opatoyinbo, O.E., Aroyewun, O.A., and Baruani, J.: Heavy
725 metals speciation and human health risk assessment at an illegal gold mining site in Igun, Osun State,
726 Nigeria, *J. Health. Pollut.*, 5, 19-32, 2015.

727 Paatero, P. and Tapper, U.: Positive matrix factorization: A non-negative factor model with optimal
728 utilization of error estimates of data values, *Environmetrics*, 5, 111-126, 1994.

729 Pacyna, J.M. and Pacyna, E.G.: An assessment of global and regional emissions of trace metals to the
730 atmosphere from anthropogenic sources worldwide, *Environ. Rev.*, 9, 269-298, 2001.

731 Prati, P., Zucchiatti, A., Lucarelli, F., Mandò, P.A.: Source apportionment near a steel plant in Genoa
732 (Italy) by continuous aerosol sampling and PIXE analysis, *Atmos. Environ.*, 34, 3149-3157, 2000.

733 Rai, P.K., Lee, S.S., Zhang, M., Tsang, Y.F., and Kim, K.: Heavy metals in food crops: Health risks, fate,
734 mechanisms, and management, *Environ. Interna.*, 125, 365-385, 2019.

735 Rasmussen, P.E.: Long-range atmospheric transport of trace metals: the need for geoscience perspectives,

736 Environ. Earth Sci., 33, 96-108, 1998.

737 Reff, A., Eberly, S.I., and Bhave, P.V.: Receptor modeling of ambient particulate matter data using
738 positive matrix factorization: review of existing methods, *J. Air Waste Manage.*, 57, 146-154, 2007.

739 Ren, Z., Zhang, B., Lu, P., Li, C., Gao, L., and Zheng, M.: Characteristics of air pollution by
740 polychlorinated dibenzo-p-dioxins and dibenzofurans in the typical industrial areas of Tangshan City,
741 China, *J. Environ. Sci. -China*, 23, 228-235, 2011.

742 Saffari, A., Daher, N., Shafer, M.M., Schauer, J.J., and Sioutas, C.: Global perspective on the oxidative
743 potential of airborne particulate matter: a synthesis of research findings, *Environ. Sci. Technol.*, 48,
744 7576-7583, 2014.

745 Shafer, M.M., Toner, B.M., Overdier, J.T., Schauer, J.J., Fakra, S.C., Hu, S., Herner, J.D., and Ayala, A.:
746 Chemical speciation of vanadium in particulate matter emitted from diesel vehicles and urban
747 atmospheric aerosols, *Environ. Sci. Technol.*, 46, 189-195, 2012.

748 Shi, G., Teng, J., Ma, H., Li, Y., and Sun, B.: Metals and metalloids in precipitation collected during
749 CHINARE campaign from Shanghai, China, to Zhongshan Station, Antarctica: Spatial variability and
750 source identification, *Global Biogeochem. Cyc.*, 29, 760-774, 2015.

751 Song, Z.F.: An assessment of the heavy metal pollution and potential ecological hazards in urban soil of
752 Tangshan City, *Geology in China* 38, 1379-1386, 2011.

753 Storelli, M.M.: Potential human health risks from metals (Hg, Cd, and Pb) and polychlorinated biphenyls
754 (PCBs) via seafood consumption : estimation of target hazard quotients (THQs) and toxic equivalents
755 (TEQs), *Food and Chemical Toxicology* 46, 2782-2788, 2008.

756 Taghvaei, S., Sowlat, M.H., Mousavi, A., Hassanvand, M.S., Yunesian, M., Naddafi, K., and Sioutas, C.:
757 Source apportionment of ambient PM_{2.5} in two locations in central Tehran using the Positive Matrix
758 Factorization (PMF) model, *Sci. Total Environ.*, 628-629, 672-686, 2018.

759 Tang, Q., Sheng, W., Li, L., Zheng, L., Miao, C., and Sun, R.: Alteration behavior of mineral structure
760 and hazardous elements during combustion of coal from a power plant at Huainan, Anhui, China,
761 *Environ. Pollut.*, 239, 768-776, 2018.

762 Tian, H., Zhu, C., Gao, J., Cheng, K., Hao, J., Wang, K., Hua, S., Wang, Y., and Zhou, J.: Quantitative
763 assessment of atmospheric emissions of toxic heavy metals from anthropogenic sources in China:
764 historical trend, spatial distribution, uncertainties, and control policies, *Atmos. Chem. Phys.*, 15,
765 10127-10147, 2015.

766 Tianxue, W., Yuesi, W., Shihyu, C., and Guangren, L.: On-line measurement of water-soluble ions in
767 ambient particles, *Adv. Atmos. Sci.*, 23, 586-592, 2006.

768 Wang, S., Su, H., Chen, C., Tao, W., Streets, D.G., Lu, Z., Zheng, B., Carmichael, G.R., Lelieveld, J.,
769 and Pöschl, U.: Natural gas shortages during the “coal-to-gas” transition in China have caused a large
770 redistribution of air pollution in winter 2017, *P. Natl. Acad. Sci. USA*, 117, 31018-31025, 2020a.

771 Wang, S., Su, H., Chen, C., Tao, W., Streets, D.G., Lu, Z., Zheng, B., Carmichael, G.R., Lelieveld, J.,
772 Pöschl, U., and Cheng, Y.: Natural gas shortages during the “coal-to-gas” transition in China have
773 caused a large redistribution of air pollution in winter 2017, *P. Natl. Acad. Sci. USA*, 117, 31018-
774 31025, 2020b.

775 Westerdahl, D., Wang, X., Pan, X., and Zhang, K.M.: Characterization of on-road vehicle emission
776 factors and microenvironmental air quality in Beijing, China, *Atmos. Environ.*, 43, 697-705,
777 <https://doi.org/10.1016/j.atmosenv.2008.09.042>, 2009.

778 Witt, M.L.I., Baker, A.R., and Jickells, T.D.: Atmospheric trace metals over the Atlantic and South Indian
779 Oceans: Investigation of metal concentrations and lead isotope ratios in coastal and remote marine

780 aerosols, *Atmos. Environ.*, 40, 5435-5451, <https://doi.org/10.1016/j.atmosenv.2006.04.041>, 2006.

781 Wu, Q., Wang, S., Zhang, L., Song, J., Yang, H., and Meng, Y.: Update of mercury emissions from China's
782 primary zinc, lead and copper smelters, 2000-2010, *Atmos. Chem. Phys.*, 12, 18207-18242,
783 <https://doi.org/10.5194/acp-12-11153-2012>, 2012.

784 Wu, Y., Wang, R., Zhou, Y., Lin, B., Fu, L., He, K., and Hao, J.: On-road vehicle emission control in
785 beijing: past, present, and future, *Environ. Sci. Technol.*, 45, 147-153,
786 <https://doi.org/10.1021/es1014289>, 2011.

787 Xiao, Q., Geng, G., Liang, F., Wang, X., Lv, Z., Lei, Y., Huang, X., Zhang, Q., Liu, Y., and He, K.:
788 Changes in spatial patterns of PM_{2.5} pollution in China 2000-2018: Impact of clean air policies,
789 *Environ. Interna.*, 141, 105776, <https://doi.org/10.1016/j.envint.2020.105776>, 2020.

790 Yang, Q., Yuan, Q., Li, T., Shen, H., and Zhang, L.: The relationships between PM_{2.5} and meteorological
791 factors in China: seasonal and regional variations, *Int. J. Env. Res. Pub. He.*, 14, 1510, 2017.

792 Yi, Y., Yang, Z., and Zhang, S.: Ecological risk assessment of heavy metals in sediment and human health
793 risk assessment of heavy metals in fishes in the middle and lower reaches of the Yangtze River basin,
794 *Environ. Pollut.*, 159, 2575-2585, <https://doi.org/10.1016/j.envpol.2011.06.011>, 2011.

795 Yu, L., Wang, G., Zhang, R., Zhang, L., Song, Y., Wu, B., Li, X., An, K., and Chu, J.: Characterization
796 and source apportionment of pm_{2.5} in an urban environment in Beijing, *Aerosol Air Qual. Res.*, 13,
797 574-583, doi: 10.4209/aaqr.2012.07.0192, 2013.

798 Zhang, J., Zhou, X., Wang, Z., Yang, L., Wang, J., Wang, W.: Trace elements in PM_{2.5} in Shandong
799 Province: Source identification and health risk assessment, *Sci. Total Environ.*, 621, 558-577, 2018.

800 Zhang, Q., Zheng, Y., Tong, D., Shao, M., Wang, S., Zhang, Y., Xu, X., Wang, J., He, H., Liu, W., Ding,
801 Y., Lei, Y., Li, J., Wang, Z., Zhang, X., Wang, Y., Cheng, J., Liu, Y., Shi, Q., Yan, L., Geng, G., Hong,
802 C., Li, M., Liu, F., Zheng, B., Cao, J., Ding, A., Gao, J., Fu, Q., Huo, J., Liu, B., Liu, Z., Yang, F., He,
803 K., and Hao, J.: Drivers of improved PM_{2.5} air quality in China from 2013 to 2017, *P. Natl. Acad. Sci.*
804 *USA*, 116, 24463-24469, <https://doi.org/10.1073/pnas.1907956116>, 2019.

805 Zhao, M., Zhang, Y., Ma, W., Fu, Q., Yang, X., Li, C., Zhou, B., Yu, Q., and Chen, L.: Characteristics
806 and ship traffic source identification of air pollutants in China's largest port, *Atmos. Environ.*, 64, 277-
807 286, <https://doi.org/10.1016/j.atmosenv.2012.10.007>, 2013.

808 Zhu, C., Tian, H., Hao, Y., Gao, J., Hao, J., Wang, Y., Hua, S., Wang, K., and Liu, H.: A high-resolution
809 emission inventory of anthropogenic trace elements in Beijing-Tianjin-Hebei (BTH) region of China,
810 *Atmos. Environ.*, 191, 452-462, <https://doi.org/10.1016/j.atmosenv.2018.08.035>, 2018.

811 Zhu, C., Tian, H., and Hao, J.: Global anthropogenic atmospheric emission inventory of twelve typical
812 hazardous trace elements, 1995-2012, *Atmos. Environ.*, 220, 117061,
813 <https://doi.org/10.1016/j.atmosenv.2019.117061>, 2020.

814

Figure 1 Topographic map of China indicating the location of Tangshan (a), the sampling site (b), and some major industrial points (b). The population distribution of Tangshan is also depicted in (b).

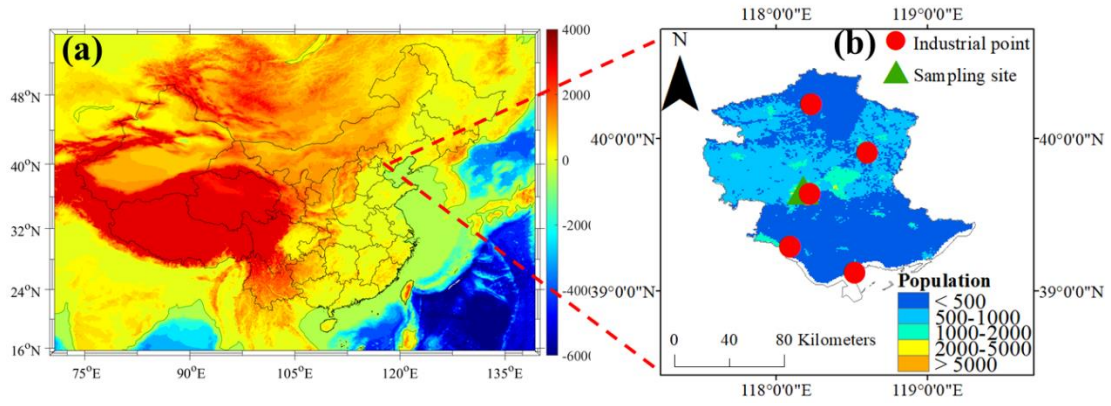


Figure 2 Bar chart of the concentrations of 16 trace elements including K, Fe, Ca, Zn, Pb, Mn, Fe, As, Se, V, Cr, Ag, Ni, Hg, Ga, and Co. The bar and black line represent mean values and associated standard deviations, respectively.

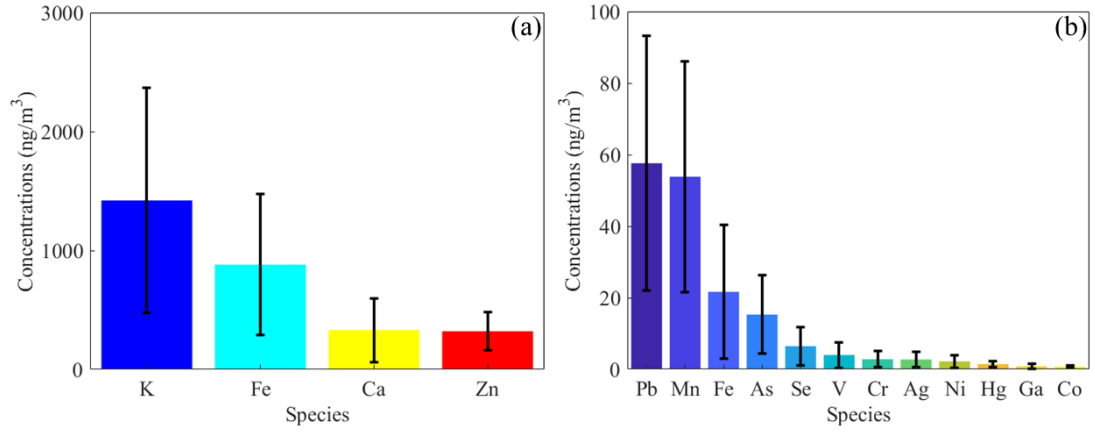


Figure 3 Inter-annual variations of the original (red) and deweathered (manganese purple) element concentrations (ng/m^3) in $\text{PM}_{2.5}$ in Tangshan. The dark, nattier blue, and nattier yellow backgrounds represent the species during 2017-2018 (from September in 2017 to August in 2018), 2018-2019 (from September in 2018 to August in 2019), and 2019-2020 (from September in 2019 to August in 2020). The bar and black line represent mean values and associated standard deviations, respectively.

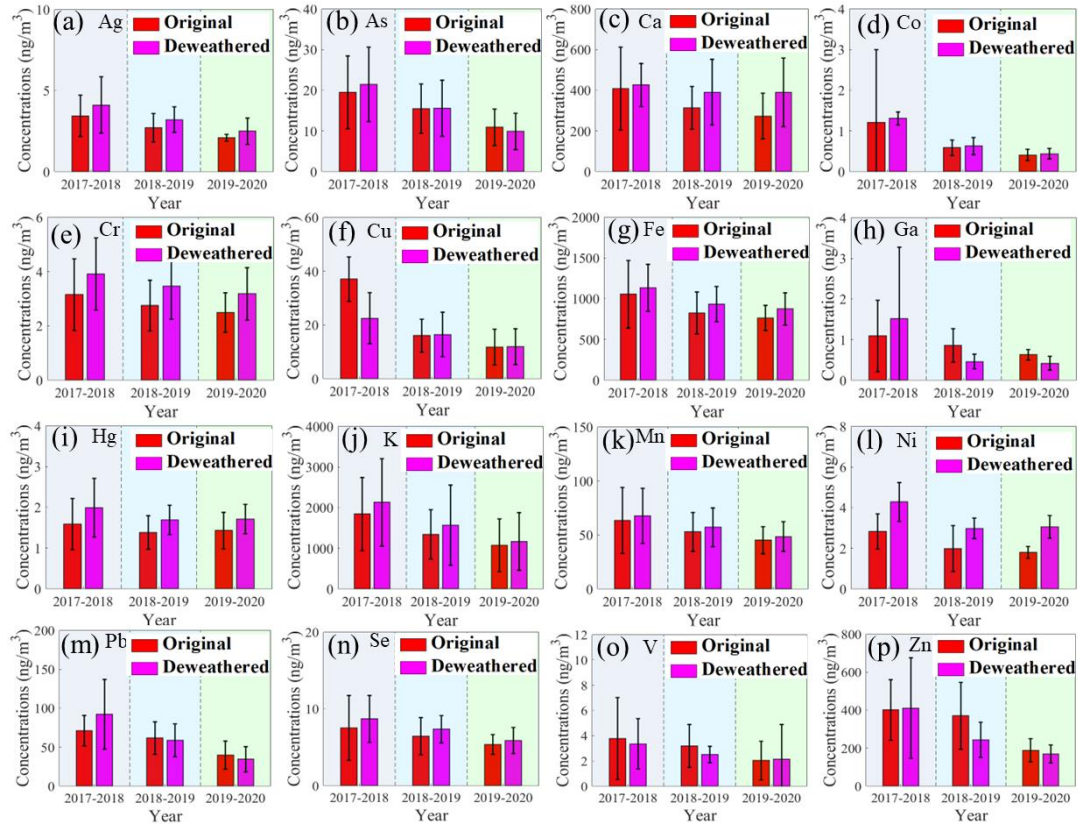


Figure 4 Original (red and orange) and deweathered (green and blue) element concentrations (ng/m^3) in $\text{PM}_{2.5}$ in Tangshan in four seasons during 2017-2018, 2018-2019, and 2019-2020. S1, U1, A1, and W1 represent the spring, summer, autumn, and winter during 2017-2018. S2, U2, A2, and W2 denote the spring, summer, autumn, and winter during 2018-2019. S3, U3, A3, and W3 are the spring, summer, autumn, and winter during 2019-2020. The point and shaded area represent mean values and associated standard deviations, respectively.

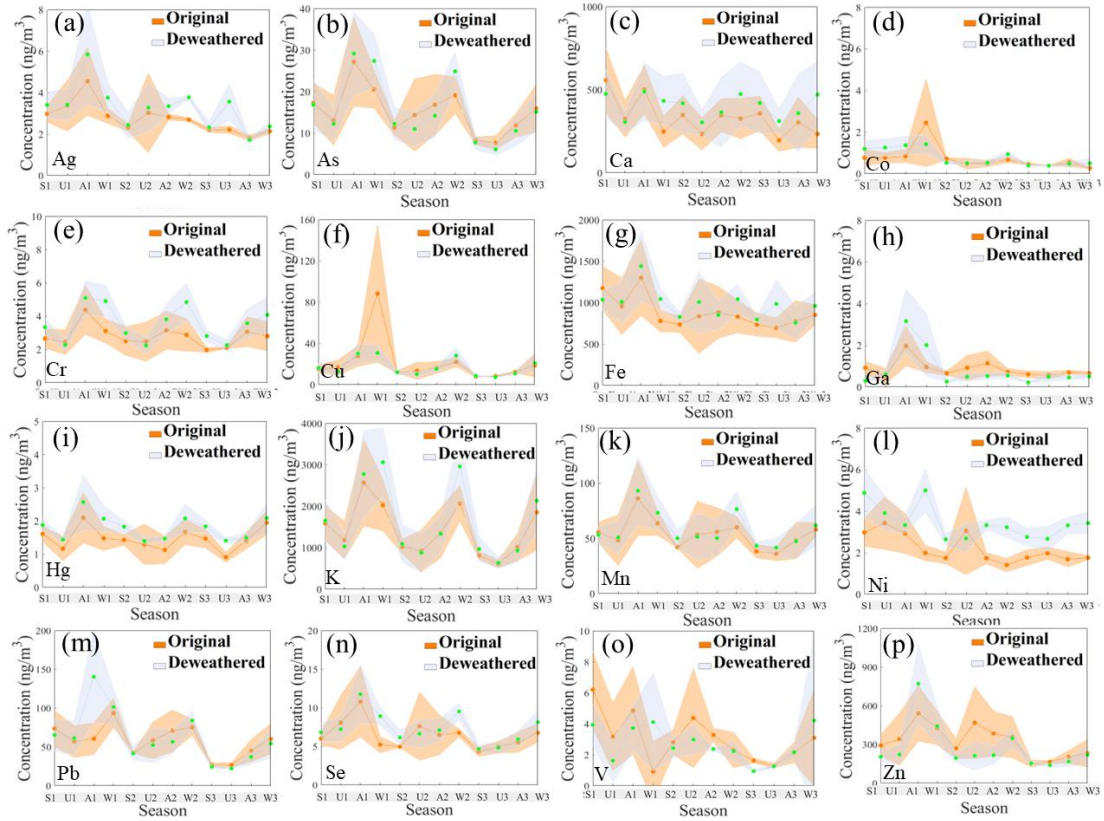


Figure 5 Weekly variations of original (green) and deweathered (orange) element concentrations (ng/m^3) in $\text{PM}_{2.5}$ in Tangshan. The green and dark backgrounds denote the error bars of original and deweathered elements, respectively. The bar and black line represent mean values and associated standard deviations, respectively.

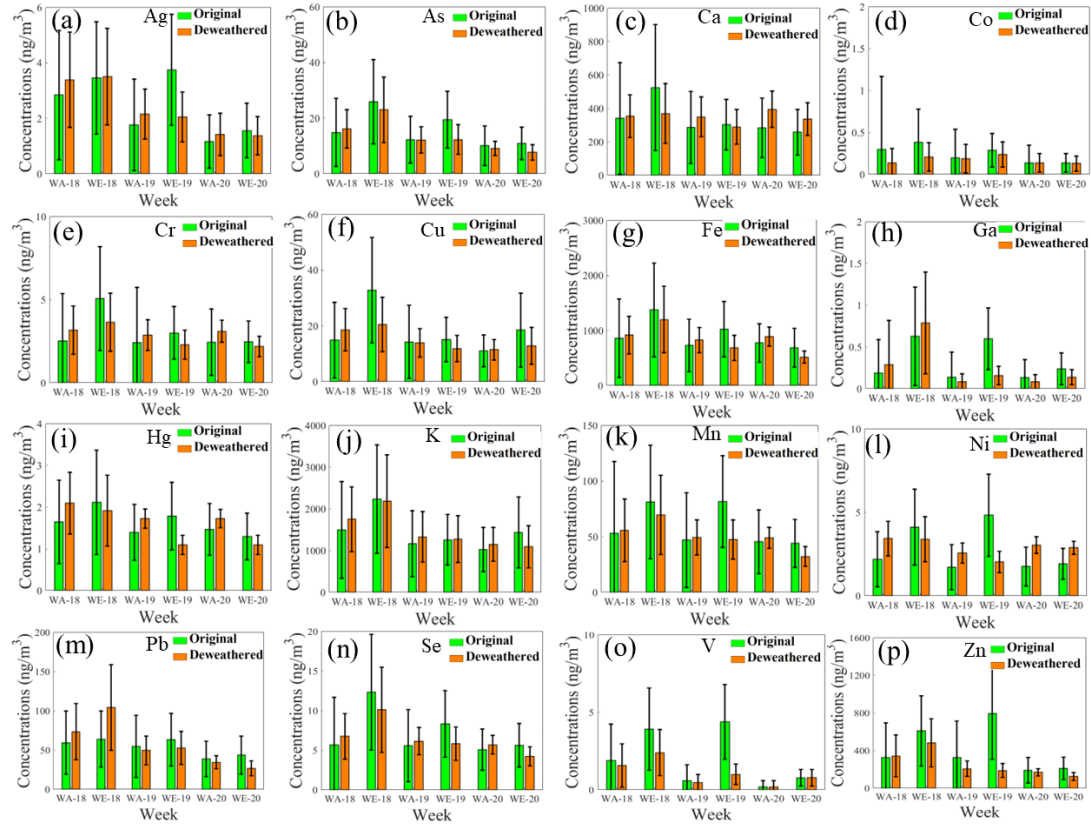


Figure 6 Relative importance of the predictors for the prediction of trace elements. The columns in the figure represent the variable importance in the RF models for the trace elements. P, RH, T, WD, WS, DOW, HOY, DOY, and Year denote air pressure, relative humidity, air temperature, wind direction, wind speed, day of week, hour of day, day of year, and study year, respectively.

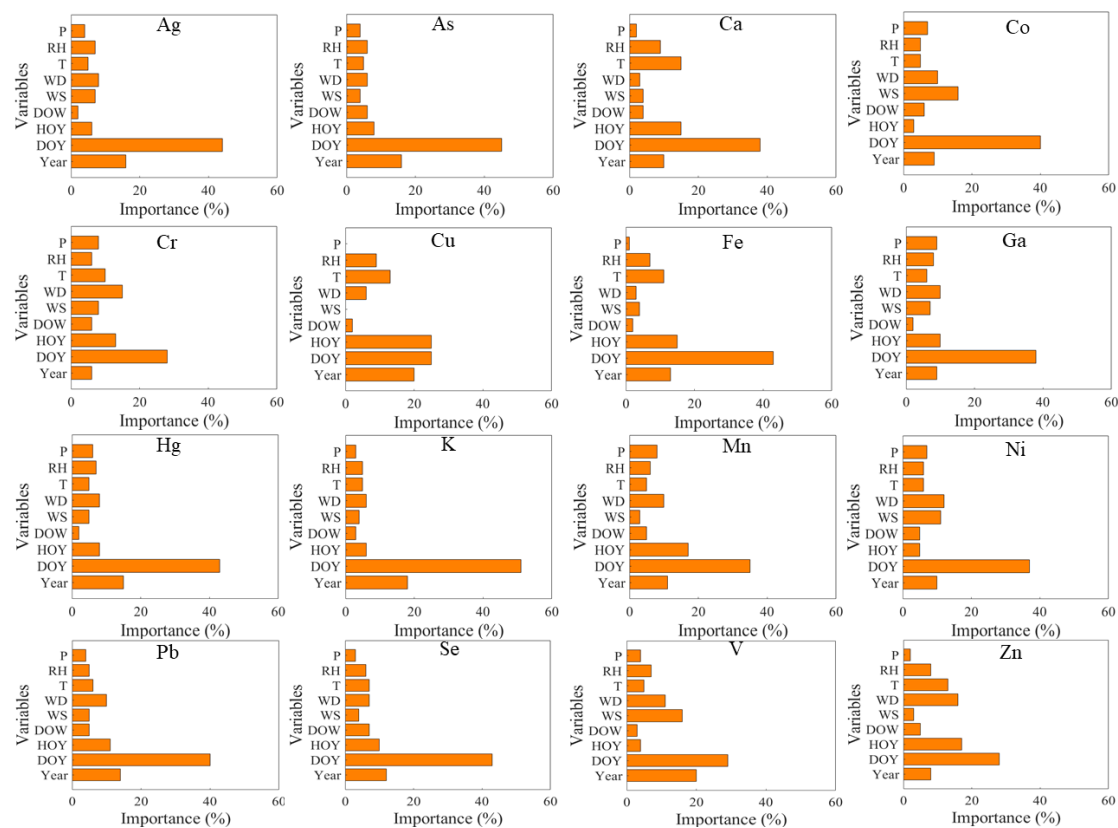


Figure 7 Deweathered concentrations of trace elements derived from six sources in Tangshan during 2017-2020.

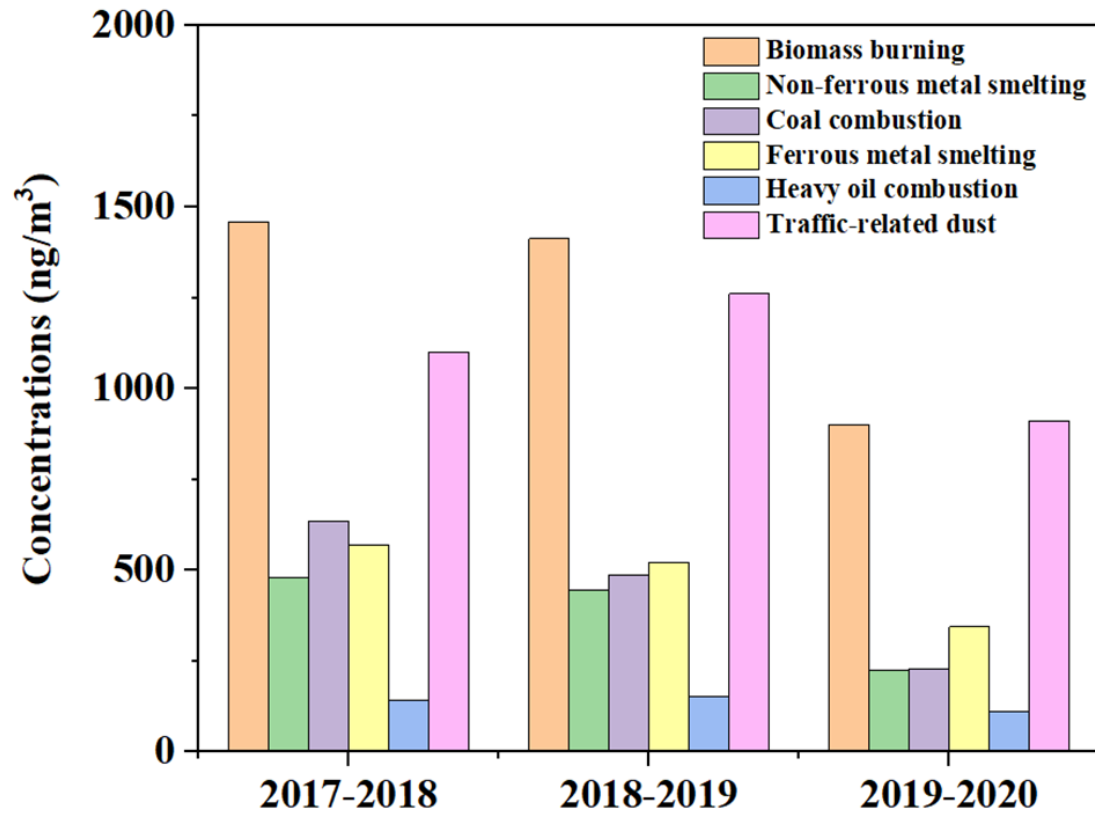


Figure 8 Average contributions of the six sources to the deweathered concentrations of elements in PM_{2.5} based on the PMF model. The red panel means the biomass burning; the green panel denotes the non-ferrous metal smelting; the blue one represents the coal combustion; the cyan one is the ferrous metal smelting; the pink one represents the heavy oil combustion; and the yellow one denotes the traffic-related dust. (a), (b), and (c) represent the source contributions during 2017-2018, 2018-2019, and 2019-2020, respectively.

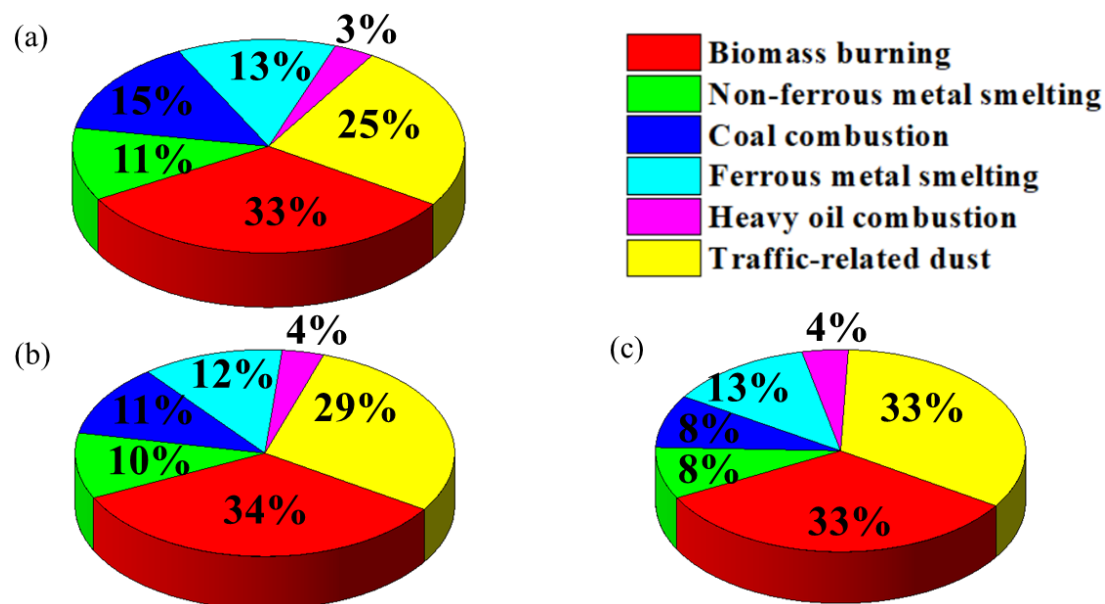


Table 1 Comparison of the element concentrations in PM_{2.5} of Tangshan and the standard values for these elements in World Health Organization (WHO), China, Europe, and the United States (Unit: ng/m³).

Elements	Mean±SD	CAAQS	WHO	EU	United States
Co	0.74±0.24				
Ga	0.86±0.74				
Hg	1.47±0.81	50	1000		
Ni	2.21±1.80		25	20	
Ag	2.75±2.08				
Cr	2.80±2.22	0.025	0.25		
V	3.98±3.57				
Se	6.46±5.28				
As	15.3±11.0	6	6.60	6	
Cu	21.7±18.7				
Mn	53.8±32.3				
Pb	57.6±35.7		1000		150
Zn	320±162				
Ca	332±268				
Fe	881 ± 591				
K	1421±947				

Table 2 Non-carcinogenic and carcinogenic risks for the original element levels in PM_{2.5}.

Age	Year	Indicator	Cr	Mn	Fe	Co	Ni	Cu	Zn	As	Pb
Adult	2017-2018	HQ	2.47×10^{-4}	1.07×10^{-4}	3.55×10^{-4}	4.50×10^{-4}	0.33×10^{-4}	1.18×10^{-4}	3.15×10^{-4}	1.53×	8.39×
	CR	0.13×10^{-6}	--	--	--	--	--	--	--	2.37×	2.88×
										10 ⁻²	10 ⁻⁴
										10 ⁻⁶	10 ⁻⁶
	2018-2019	HQ	2.16×10^{-4}	0.89×10^{-4}	2.77×10^{-4}	4.67×10^{-4}	0.23×10^{-4}	0.95×10^{-4}	2.91×10^{-4}	1.21×	7.28×
CR	0.11×10^{-6}	--	--	--	--	--	--	--	1.87×	2.50×	
									10 ⁻²	10 ⁻⁴	
									10 ⁻⁶	10 ⁻⁶	
2019-2020	HQ	1.95×10^{-4}	0.76×10^{-4}	2.58×10^{-4}	3.26×10^{-4}	0.21×10^{-4}	0.70×10^{-4}	1.49×10^{-4}	0.86×	4.69×	
CR	0.10×10^{-6}	--	--	--	--	--	--	--	1.33×	1.61×	
									10 ⁻²	10 ⁻⁴	
									10 ⁻⁶	10 ⁻⁶	
Child	2017-2018	HQ	6.02×10^{-4}	2.60×10^{-4}	8.64×10^{-4}	11.1×10^{-4}	0.81×10^{-4}	2.87×10^{-4}	7.67×10^{-4}	3.73×	20.4×
	CR	0.08×10^{-6}	--	--	--	--	--	--	--	1.44×	1.75×
										10 ⁻²	10 ⁻⁴
										10 ⁻⁶	10 ⁻⁶
	2018-2019	HQ	5.26×10^{-4}	2.17×10^{-4}	6.74×10^{-4}	11.0×10^{-4}	0.57×10^{-4}	2.30×10^{-4}	7.08×10^{-4}	2.95×	17.7×
CR	0.07×10^{-6}	--	--	--	--	--	--	--	1.14×	1.52×	
									10 ⁻²	10 ⁻⁴	
									10 ⁻⁶	10 ⁻⁶	

2019-2020	HQ	4.75×10^{-4}	1.85×10^{-4}	6.27×10^{-4}	7.93×10^{-4}	0.52×10^{-4}	1.70×10^{-4}	3.61×10^{-4}	2.09×10^{-2}	11.4×10^{-4}
	CR	0.06×10^{-6}	--	--	--	--	--	--	0.81×10^{-6}	0.98×10^{-6}

Table 3 Non-carcinogenic and carcinogenic risks for the deweathered element levels in PM_{2.5}.

Age	Year	Indicator	Cr	Mn	Fe	Co	Ni	Cu	Zn	As	Pb
Adult	2017-2018	HQ	3.07×10^{-4}	1.14×10^{-4}	3.82×10^{-4}	10.3×10^{-4}	0.50×10^{-4}	1.33×10^{-4}	3.15×10^{-4}	1.68×	10.8×
										10 ⁻²	10 ⁻⁴
		CR	0.16×10^{-6}	--	--	--	--	--	--	2.60×	3.72×
										10 ⁻⁶	10 ⁻⁶
	2018-2019	HQ	2.73×10^{-4}	0.96×10^{-4}	3.14×10^{-4}	4.93×10^{-4}	0.35×10^{-4}	0.97×10^{-4}	2.91×10^{-4}	1.22×	6.91×
										10 ⁻²	10 ⁻⁴
	CR	0.14×10^{-6}	--	--	--	--	--	--	1.89×	2.37×	
									10 ⁻⁶	10 ⁻⁶	
2019-2020	HQ	2.50×10^{-4}	0.82×10^{-4}	2.95×10^{-4}	3.46×10^{-4}	0.36×10^{-4}	0.70×10^{-4}	1.49×10^{-4}	0.78×	4.08×	
									10 ⁻²	10 ⁻⁴	
	CR	0.13×10^{-6}	--	--	--	--	--	--	1.20×	1.40×	
									10 ⁻⁶	10 ⁻⁶	
Child	2017-2018	HQ	7.47×10^{-4}	2.77×10^{-4}	9.28×10^{-4}	11.7×10^{-4}	1.23×10^{-4}	3.22×10^{-4}	3.23×10^{-4}	4.09×	26.4×
										10 ⁻²	10 ⁻⁴
		CR	0.10×10^{-6}	--	--	--	--	--	--	1.58×	2.26×
										10 ⁻⁶	10 ⁻⁶
	2018-2019	HQ	6.64×10^{-4}	2.34×10^{-4}	7.64×10^{-4}	11.9×10^{-4}	0.85×10^{-4}	2.36×10^{-4}	1.91×10^{-4}	2.98×	16.8×
										10 ⁻²	10 ⁻⁴
	CR	0.09×10^{-6}	--	--	--	--	--	--	1.15×	1.44×	
									10 ⁻⁶	10 ⁻⁶	

2019-2020	HQ	6.08×10^{-4}	1.99×10^{-4}	7.17×10^{-4}	8.42×10^{-4}	0.87×10^{-4}	1.71×10^{-4}	1.34×10^{-4}	1.89×	9.92×
									10^{-2}	10^{-4}
	CR	0.08×10^{-6}	--	--	--	--	--	--	0.73×	0.85×
									10^{-6}	10^{-6}
